

BUNCHED BEAM COHERENT INSTABILITIES

J.L. Laclare
Laboratoire National Saturne, 91191 Gif-sur-Yvette Cedex, France

ABSTRACT

In this chapter, we will deal with coherent longitudinal and transverse instabilities. It is a collective phenomenon which prevents one from increasing the current circulating in an accelerating device without losing the beam or spoiling its characteristics.

1. INTRODUCTION

The origin of the mechanism is the electromagnetic field created by the beam itself. This self-field is proportional to the beam intensity. Furthermore, like any solution of Maxwell's equations, because of boundary conditions, it depends strongly on the geometry and the electromagnetic properties of the environment. When the intensity gets large enough, it becomes sizeable in the sense that it cannot be neglected anymore when compared to the external guide field.

Dealing with coherent instabilities consists in solving the equation of motion of a population of particles while adding the self-field effect. Obviously, the self field perturbs the single particle motion, but this is not the remarkable effect. The important point is that under certain conditions the beam as a whole is unstable.

In literature, there is a countless list of contributions to the subject. The first to come have been written in the fifties. Nowadays, the subject is still in fashion. Many reports per year are being produced. This shows how difficult and important the subject is.

During these two chapters, I will review the fundamentals of coherent instabilities. In this respect, F. Sacherer's work is certainly the basic source. The main material for this chapter is drawn from the numerous reports he wrote about ten years ago. Numerous developments are derived from B. Zotter and G. Besnier's contributions.

In the following, we will only study bunched beams in circular machines; first longitudinal and then transverse motion.

2. LONGITUDINAL INSTABILITIES

2.1 Single particle longitudinal motion

With respect to the synchronous particle that circulates at the angular revolution frequency

$$\omega_0 = \frac{pc}{R} \quad (1)$$

and crosses the Radio Frequency gap when the RF phase is ψ_s , we describe the single particle motion with a pair of conjugate coordinates

$$\tau \quad \text{and} \quad \dot{\tau} = \frac{d\tau}{dt} . \quad (2)$$

For a fixed observer located at azimuthal position θ around the machine, τ expressed in seconds represents the time interval between the reference particle passing and the test particle passing. The second coordinate

$$\dot{\tau} = \gamma \frac{dp}{p_{\parallel}} = - \frac{d\omega}{\omega_0} \quad (3)$$

measures the instantaneous momentum deviation of the test particle. The parameter γ is negative below the transition energy.

$$\eta = \frac{1}{\gamma_t^2} - \frac{1}{\gamma^2} . \quad (4)$$

In smooth machines γ_t is of the order of Q_x (horizontal wave number).

We assume a purely linear synchrotron oscillation around the synchronous particle at frequency ω_{so} .

$$\ddot{\zeta} + \omega_{so}^2 \zeta = 0 \quad (5)$$

$$\omega_{so}^2 = \frac{-\eta \omega_0 V_{RF} h \cos \varphi_s}{2\pi R \left(\frac{P_{\parallel}}{e} \right)} \quad (6)$$

e is the elementary charge
 R the machine radius
 P_{\parallel} the synchronous particle momentum
 V_{RF} the peak RF voltage
 h the RF harmonic number

In $(\zeta, \dot{\zeta})$ phase space the trajectory associated with the unperturbed motion is an ellipse (Fig. 1a).

$$\zeta^2 + \frac{\dot{\zeta}^2}{\omega_{so}^2} = \frac{1}{2} = \frac{\eta^2}{\omega_{so}^2} \left(\frac{dp}{P_{\parallel}} \right)^2 . \quad (7)$$



Fig. 1 Synchrotron motion in phase space. a) Phase space $(\zeta, \dot{\zeta})$
b) Normalised phase space $(\zeta, \dot{\zeta}/\omega_{so})$ or $(\hat{\zeta}, \psi)$

This ellipse becomes a circle when using a set of normalized coordinates like ζ , $\dot{\zeta}/\omega_{so}$ or phase and amplitude coordinates ψ , $\hat{\zeta}$ (Fig. 1b).

As stated from the beginning, we are mainly concerned with the electromagnetic field induced by the beam. This field has electric and magnetic components. It modifies the differential equation of motion (5) of the single particle by adding a term in the right hand side of the equation

$$\ddot{\zeta} + \omega_{so}^2 \zeta = \frac{\eta}{P_{\parallel}} \frac{dP_{\parallel}}{dt} = \frac{\eta}{P_{\parallel}} e \left[\vec{E} + \vec{B} \times \vec{v} \right]_{\parallel} (t, \theta) . \quad (8)$$

2.2 Single-particle longitudinal signal

With the object of writing down Maxwell's equations the solution of which leads to the beam self-field, one needs to express the local charge and current at time t and position θ in the machine. Machine physicists are used to observing the intensity on an oscilloscope by looking at the signal drawn from longitudinal P U electrodes. These electrodes are non-destructive diagnostic equipments which measure the electromagnetic field locally induced by the beam.

Let us assume a perfect P U electrode located at angular azimuth θ , and analyse the intensity signal when a single test particle oscillates in the external guide field (no self field added). This will help us to get more familiar with time domain and frequency domain.

In the time domain, the elementary intensity signal $s_{\parallel}(t, \theta)$ is a series of nearly periodical impulses delivered at each passage through the electrode.

$$s_{\parallel}(t, \theta) = e \sum_{k=-\infty}^{k=\infty} \delta(t - \tau - \frac{\theta}{\omega_0} - 2k\pi) \quad \text{Ampere} \quad (9)$$

δ is the Dirac function.

By using the following relations,

$$u = t - \tau - \frac{\theta}{\omega_0} \quad \sum_{k=-\infty}^{k=\infty} \delta(u - k \frac{2\pi}{\omega_0}) = \frac{\omega_0}{2\pi} \sum_{p=-\infty}^{p=\infty} e^{j p \omega_0 u} \quad (10)$$

$$\tau = \hat{\tau} \cos(\omega_{s_0} t + \psi_0) \quad (11)$$

$$e^{-j p \omega_0 \hat{\tau}} \cos(\omega_{s_0} t + \psi_0) = \sum_{m=-\infty}^{m=\infty} j^m J_m(p \omega_0 \hat{\tau}) e^{j m (\omega_{s_0} t + \psi_0)} \quad (12)$$

where ψ_0 is the synchrotron phase at time $t=0$
it can be rewritten in the equivalent form

$$s_{\parallel}(t, \theta) = \frac{e \omega_0}{2\pi} \sum_{p,m=-\infty}^{p,m=\infty} j^m J_m(p \omega_0 \hat{\tau}) e^{j(\omega_{pm} t - p\theta + m\psi_0)} \quad (13)$$

in which $\omega_{pm} = p \omega_0 + m \omega_{s_0}$. (14)

The Fourier transform of the elementary signal is given by

$$s_{\parallel}(\omega, \theta) = \frac{1}{2\pi} \int_{t=-\infty}^{t=\infty} s_{\parallel}(t, \theta) e^{-j \omega t} dt. \quad (15)$$

With the Fourier transform we can pass on to frequency domain. The actual spectrum of our single particle moving in the external guide field is a line spectrum at frequencies ω_{pm}

$$s_{\parallel}(\omega, \theta) = \frac{e \omega_0}{2\pi} \sum_{p,m=-\infty}^{p,m=\infty} j^m J_m(p \omega_0 \hat{\tau}) e^{-j(p\theta - m\psi_0)} \delta(\omega - \omega_{pm}). \quad (16)$$

Around every harmonic of the revolution frequency, there is an infinite number of synchrotron satellites. The spectral amplitude of the m th satellite is given by $J_m(p \omega_0 \hat{\tau})$ (Bessel function of order m). The spectrum is centered at the origin and spreads in the negative and in the positive frequency domain. Because the argument of the Bessel functions is proportional to $\hat{\tau}$, the width of the spectrum behaves like $(\hat{\tau})^m$. As a consequence, when considering a bunch, particles with small (large) synchrotron amplitude contribute to the high (low) frequency part of the spectrum. At the limit $\hat{\tau} \rightarrow 0$, the synchrotron satellites disappear. The synchronous particle resumes the observation point periodically. Its spectrum is a line spectrum at harmonics of the revolution frequency.

$$s_{\parallel}(\omega, \theta) = \frac{e \omega_0}{2\pi} \sum_{p=-\infty}^{p=\infty} J_0(p \omega_0 \hat{\tau}) e^{-j p \theta} \delta(\omega - p \omega_0) \quad (17)$$

2.3 Distribution of particles

The next step consists in gathering particles to form a bunch (a single bunch for the moment). Therefore we have to choose a distribution function $\Psi(\psi_0, \hat{\tau}, t)$ which will

indicate the particle density in phase space.

The signal or the electromagnetic field induced on the P U electrode by the entire beam is obtained by summing up the elementary signal of individual particles over the distribution.

$$S_{\parallel}(\epsilon, \theta) = N \int_{\psi_0=0}^{\psi_0=2\pi} \int_{\hat{z}=0}^{\hat{z}=\infty} \Psi(\psi_0, \hat{z}, \epsilon) s_{\parallel}(\epsilon, \theta) \hat{z} d\hat{z} d\psi_0. \quad (18)$$

where N is the number of particles per bunch.

For obvious reasons of normalization, Ψ has to satisfy equation (19)

$$\int \Psi dv = 1 \quad (19)$$

2.3.1 Stationary distribution of particles

First, let us consider a stationary distribution, that is to say a distribution that depends on ϵ solely.

$$\Psi(\psi_0, \hat{z}, \epsilon) = g_0(\hat{z}). \quad (20)$$

For such a distribution, as it was already the case for the synchronous particle, the frequency spectrum of the electromagnetic field induced on the P U electrode is a line spectrum at harmonics of the revolution frequency.

$$S_{\parallel}(\omega, \theta) = 2\pi I \sum_{p=-\infty}^{p=+\infty} \delta(\omega - p\omega_0) e^{ip\theta} \left(\int_{\hat{z}=0}^{\hat{z}=\infty} J_0(p\omega_0 \hat{z}) g_0(\hat{z}) \hat{z} d\hat{z} \right) \quad (21)$$

where I is the intensity in one bunch.

$$I = \frac{N e \omega_0}{2\pi}. \quad (22)$$

The amplitude of the spectrum at frequency $p\omega_0$ is given by

$$\sigma_0(p) = \int_{\hat{z}=0}^{\hat{z}=\infty} J_0(p\omega_0 \hat{z}) g_0(\hat{z}) \hat{z} d\hat{z}. \quad (23)$$

There is no synchrotron satellite and therefore no evidence at all of an internal synchrotron motion. Turn after turn, each small volume of synchrotron phase space that rotates at fixed distance from the synchronous particle is replaced by an equivalent volume with the same density.

The stationary distribution gives the average density. It can be adapted to simulate different types of bunches.

A few typical examples are given hereunder. In these examples, τ_L represents the full bunch length (or 4 standard deviations in the gaussian case). To make the writing easier, the dimensionless variables

$$Z = \frac{z}{\tau_L} \quad \hat{Z} = \frac{\hat{z}}{\tau_L} \quad \text{and} \quad B = \frac{\omega_0 \tau_L}{2\pi} \quad (\text{bunching factor}) \quad (24)$$

are used.

- Parabolic amplitude density ($0 < \hat{z} < 1$)

$$q_o(\hat{z}) = \frac{2}{\pi \left(\frac{\tau_L}{z} \right)^2} (1 - \hat{z}^2) ; \lambda(z) = \frac{8}{3\pi \left(\frac{\tau_L}{z} \right)} (1 - z^2)^{\frac{3}{2}} ; S_{\infty o}(\omega, \theta) = 8I \sum_p \delta(\omega - p\omega_o) e^{-jp\theta} \frac{J_2(p\pi B)}{(p\pi B)^2} \quad (25)$$

- Parabolic line density suitable for proton bunches ($0 < \hat{z} < 1$)

$$q_o(\hat{z}) = \frac{3}{2\pi \left(\frac{\tau_L}{z} \right)^2} (1 - \hat{z}^2)^{\frac{1}{2}} ; \lambda(z) = \frac{3}{4 \left(\frac{\tau_L}{z} \right)} (1 - z^2) ; S_{\infty o}(\omega, \theta) = 3I \sum_p \delta(\omega - p\omega_o) e^{-jp\theta} \sqrt{\frac{\pi}{2}} \frac{J_{\frac{3}{2}}(p\pi B)}{(p\pi B)^{\frac{3}{2}}} \quad (26)$$

- Gaussian amplitude density suitable for electron bunches ($0 < \hat{z} < \infty$)

$$q_o(\hat{z}) = \frac{2}{\pi \left(\frac{\tau_L}{z} \right)^2} e^{-2\hat{z}^2} ; \lambda(z) = \sqrt{\frac{2}{\pi}} \frac{1}{\left(\frac{\tau_L}{z} \right)} e^{-2z^2} ; S_{\infty o}(\omega, \theta) = I \sum_p \delta(\omega - p\omega_o) e^{-jp\theta} e^{-\frac{(p\pi B)^2}{8}} \quad (27)$$

- "Water bag" bunch ($0 < \hat{z} < 1$)

$$q_o(\hat{z}) = \frac{1}{\pi \left(\frac{\tau_L}{z} \right)^2} ; \lambda(z) = \frac{2}{\pi \left(\frac{\tau_L}{z} \right)} (1 - z^2)^{\frac{1}{2}} ; S_{\infty o}(\omega, \theta) = 2I \sum_p \delta(\omega - p\omega_o) e^{-jp\theta} \frac{J_1(p\pi B)}{p\pi B} \quad (28)$$

The line density $\lambda(\tau)$ is the projection of the distribution $q_o(\hat{z})$ on the τ axis.

$$\lambda(\tau) = \int q_o(\hat{z}) \frac{d\hat{z}}{\omega_s} \quad \int \lambda(\tau) d\tau = 1 \quad (29)$$

The corresponding power spectra $|S_{\infty o}(\omega, \theta)|^2$ (Fig. 2a) and single pass signals (Fig. 2b) are drawn for comparison. The spectrum is peaked at zero frequency and extends $\pm 2\pi/\tau_L$ rad/sec.

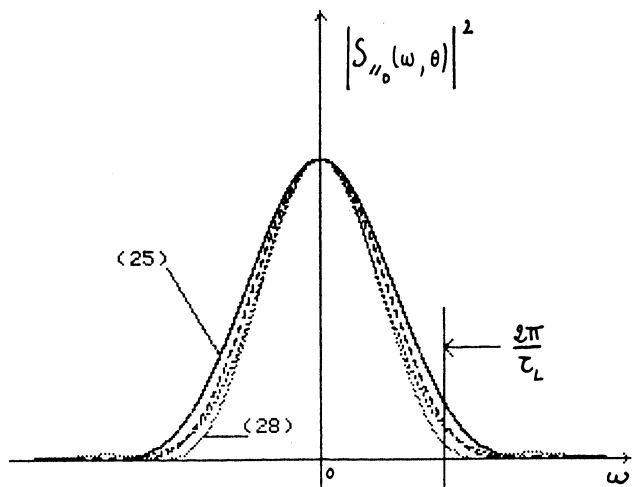


Fig. 2(a) Power spectra for various particle distributions

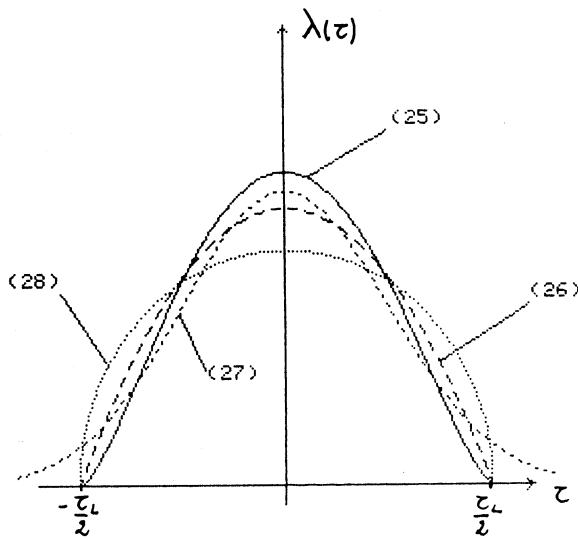


Fig. 2(b) Line densities for the various particle distributions of Fig. 2(a)

As will be pointed out later on, in Vlasov's equation, for the longitudinal case, the quantity of interest is $\frac{d\phi_0/dt}{dt}$ or $\frac{d\lambda/d\tau}{d\tau}$. In this respect, the choice of distributions like the "water bag" distribution must be avoided. As a matter of fact, it shows a sharp discontinuity at its edge that leads to unrealistic results since it attaches too much importance to large amplitude particles.

In the rest of this lecture on longitudinal instabilities, we will mainly use the distribution with parabolic amplitude density. On one hand, it is a good compromise between proton and electron bunches. On the other hand, according to my own experience, the three realistic distributions listed above lead to results that do not deviate by more than 20%.

The electromagnetic field induced by the stationary distribution is at harmonics of the revolution frequency. As a consequence, it acts on the beam as the external RF system does. First it is responsible for synchronous phase shift. Then, it can depress or increase the focusing. It can also introduce non linear terms because of the rich harmonic content of the spectrum.

Nevertheless, the internal synchrotron motion of individual particles is hidden and one cannot expect any excitation of coherent motion without any force at harmonics of the synchrotron frequency. So, we need a new ingredient in order to get a scenario of initial conditions that can lead to instability.

2.3.2 Perturbation

This ingredient consists in a distribution $\Delta\Psi(\psi_0, \hat{\tau}, t)$ which has the property of introducing some electromagnetic field at harmonics of the synchrotron frequency. It is a density perturbation which represents the difference between the actual beam and the stationary distribution. As a matter of fact, in terms of physics, a stationary beam does not exist. On one hand, there is always some density modulation that remains from previous beam manipulations such as injection, bunching, etc... On the other hand, the bunch is composed of individual particles, each of them gives a rich spectrum including synchrotron sidebands. On an average, we get a stationary bunch. Nevertheless, there is always some remaining noise at synchrotron satellite frequencies.

The form that can be given to $\Delta\Psi$ is suggested by the single particle signal (13) and (16). In phase space, on a given orbit $\hat{\tau}$, one can choose the initial ψ_0 dependence of the charge density in order to enhance the signal amplitude at a given harmonic of the synchrotron frequency.

For instance, with

$$\Delta\Psi(\psi_0, \hat{\tau}, t) = g_m(\hat{\tau}) e^{j m \psi_0} e^{j \Delta_{cm} t} \quad m \neq 0 \quad (30)$$

(the assumed time dependence of the perturbation will be justified at the end of this section) one gets a perturbation signal

$$\Delta S_{\parallel m}(\omega, \theta) = 2\pi I \sum_p \delta(\omega - (p\omega_0 + m\omega_s + \Delta\omega_{cm})) \int_{\hat{z}=0}^{\hat{z}=\infty} J_m(p\omega_0 \hat{z}) q_m(\hat{z}) \hat{z} d\hat{z}. \quad (31)$$

Therefore, owing to the $e^{-im\psi_0}$ charge density, the spectral amplitude is maximum for satellite number m and null for all other satellites.

We have defined a perturbation which is coherent with respect to satellite number m . The amplitude of the perturbation spectrum at frequency $\omega = p\omega_0 + m\omega_s + \Delta\omega_{cm}$ is given by

$$\sigma_m(p) = \int_{\hat{z}=0}^{\hat{z}=\infty} J_m(p\omega_0 \hat{z}) q_m(\hat{z}) \hat{z} d\hat{z} \quad (32)$$

In order to give more physical content to the expression of the perturbation (30), let us imagine an injection scheme in which a bunch is transferred from a booster to a main ring.

After transfer, when ideal conditions are fulfilled, the bunch is perfectly matched and individual particles continue their motion on the "same" phase space orbit.

Now, let us assume a RF phase error or an energy error at transfer. Then, in phase space, the beam center of mass rotates around the main ring synchronous orbit (Fig. 3a). Triggered by the RF clock, the PU signal shows that the bunch is oscillating forwards and backwards (Fig. 3b). When compared to the ideal transfer (stationary bunch) a density perturbation of $\cos \psi_0$ ($e^{-im\psi_0}$ with $m=1$) type has been added. It corresponds to an excess of charges at one bunch edge, exactly balanced by a lack of charges at the opposite edge.

Using instability terminology, a coherent dipolar perturbation has been induced.

If one neglects the electromagnetic self-field influence, then, this figure rotates at frequency ω_{so} in phase space. The power spectrum of the signal has two components, the spectrum of the stationary distribution at harmonics of the revolution frequency and the spectrum induced by the perturbation at $p\omega_0 + \omega_{so}$. This last component is peaked at higher frequency $\omega \sim 2\pi/\tau_L$ since it represents details with short wavelength occurring during the bunch passing τ_L .

If one takes the electromagnetic self-field into account, then, two major effects are expected.

- Firstly, we will get a shift of the synchrotron frequency ω_{so} . The field induced by the stationary distribution at $p\omega_0$ acts on the beam like an RF system does. It modifies the external focusing. This shift

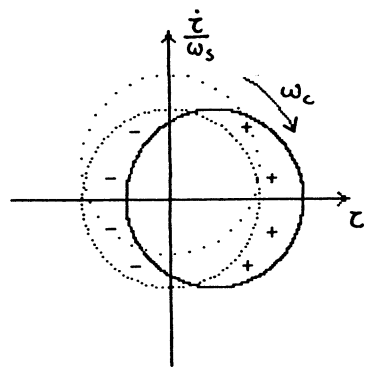
$$\Delta\omega_i = \omega_s - \omega_{so} \quad (33)$$

will be called incoherent synchrotron frequency shift.

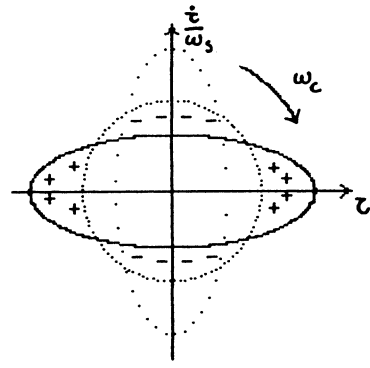
- Secondly, the perturbation will not rotate at the incoherent synchrotron frequency ω_s , but at the coherent frequency ω_c , $\Delta\omega_{c1}$ apart.

$$\Delta\omega_{c1} = \omega_c - \omega_s. \quad (34)$$

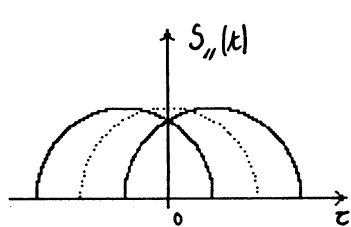
This is the reason why the $e^{i\Delta\omega_{c1}\tau}$ term has been introduced in equation (30) already. At the same time ω_{so} has been replaced by ω_s .



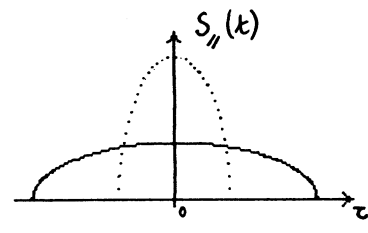
a)



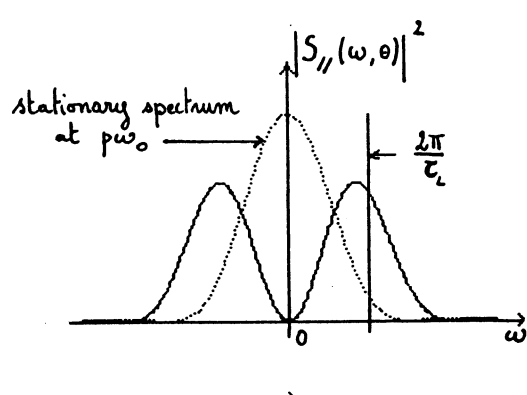
a)



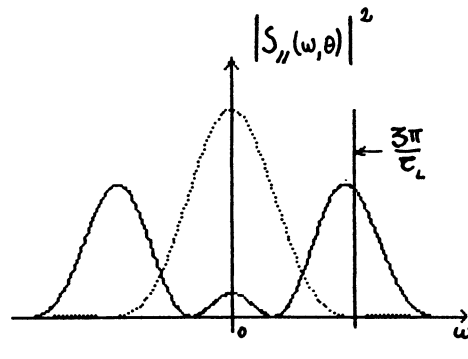
b)



b)



c)



c)

Fig. 3 Dipole mode of longitudinal bunch oscillations

- a) Phase-plane diagram
- b) Line density as seen on a pick-up
- c) Frequency spectrum for the dipole/quadrupole mode

Fig. 4 Quadrupole mode of longitudinal bunch oscillations

$\Delta\omega_{ci}$ is called coherent frequency shift.

The line spectrum of the perturbation which was at $p\omega_0 + \omega_{so}$ for zero current, is now at $p\omega_0 + \omega_c$.

The goal we aim at consists in finding out the expression of both quantities $\Delta\omega_i$ and $\Delta\omega_{cm}$. We will assume that $\Delta\omega_{cm}$ is a complex number. Its real part will give us the real coherent frequency shift. The sign of its imaginary part will tell us whether the initial perturbation will grow ($I_m(\Delta\omega_{cm}) < 0$ instability) or will be damped ($I_m(\Delta\omega_{cm}) > 0$ stability).

As a second example, let us describe a coherent quadrupolar perturbation. One can assume an error of RF voltage in the main ring. In this case, because of the focusing mismatching, the transferred beam has an elliptical shape in main ring phase (Fig. 4a). This corresponds to a $\cos 2\psi_0$ ($e^{-j\pi m\psi_0}$ with $m=2$) density perturbation. The ellipse has a twofold symmetry in phase space. It repeats at the coherent frequency ω_c , that is to say at twice the incoherent synchrotron frequency ω_s plus the coherent frequency shift $\Delta\omega_{c2}$.

$$\Delta\omega_{c2} = \omega_c - 2\omega_s . \quad (35)$$

Since we have to describe more and more details during the bunch passing τ_L , the perturbation signal is peaked at higher frequency again $\omega \sim 3\pi/\tau_L$ (Fig. 4c). The electromagnetic field induced by the perturbation is at

$$p\omega_0 + \omega_c \quad -\infty < p < +\infty \quad (36)$$

$$\omega_c = 2\omega_{so} \text{ for zero current and } \omega_c = 2\omega_s + \Delta\omega_{c2} \text{ for } I \neq 0 .$$

There is an infinite number of possible coherent perturbations

$m=1$	dipole
$m=2$	quadrupole
$m=3$	sextupole, etc...

For zero intensity,

$$\omega_{cm} = m\omega_{so} \quad (37)$$

the frequency separation between two adjacent coherent perturbations is ω_{so} .

For $I \neq 0$,

$$\omega_{cm} = m\omega_s + \Delta\omega_{cm} \quad (38)$$

one can distinguish two regimes.

In the low intensity regime, the basic frequency separation is not ω_{so} but ω_s the incoherent synchrotron frequency. It has been slightly changed by the effect of the electromagnetic field at $p\omega_0$ arising from the stationary distribution $\Delta\omega_i = \omega_s - \omega_{so} \ll \omega_{so}$. In parallel, the coherent frequency shift remains small $\Delta\omega_{cm} \ll \omega_{so}$. Therefore, the coherent frequencies of two adjacent perturbations are still well separated and one can study each of the perturbations separately while restricting to a single value of m .

$$\Delta\Psi = g_m(z) e^{-j\pi m\psi_0} e^{\int \Delta\omega_{cm} t} \quad (30)$$

In the high intensity regime, the coherent and incoherent shifts get large and the frequencies associated with two adjacent perturbations m and $m+1$ can get very close. As a consequence, one has to sum up several values of m in the $\Delta\Psi$ expression.

$$\Delta \Psi = \sum_m q_m(\hat{\epsilon}) e^{-j^m \Psi_0} e^{j \Delta \omega_{cm} t}. \quad (39)$$

2.4 Longitudinal coupling impedance

All the properties of the electromagnetic response of a given machine to the beam passings are gathered into a key parameter, the so called longitudinal coupling impedance $Z_{\parallel}(\omega)$. It allows one to predict the self field acting along the beam axis in terms of signal.

$$2\pi R [\vec{E} + \beta c \wedge \vec{B}]_{\parallel}(t, \theta) = - \int_{\omega=-\infty}^{\omega=+\infty} Z_{\parallel}(\omega) S_{\parallel}(\omega, \theta) e^{j\omega t} d\omega \quad (40)$$

Z_{\parallel} is expressed in ohm.

If $Z_{\parallel}(\omega)$ were a constant independent of frequency, then, the self-field would be proportional to the signal. This explains the close connection that has been made between signal and self field up to now. We will avoid undertaking a detailed justification of equation (40) since it has been done in the basic lecture given last year already. We will limit ourselves to a qualitative discussion of the solution of Maxwell's equation applied to the crude model of a round beam of radius a travelling on axis in a circular pipe of radius b (Fig. 5).

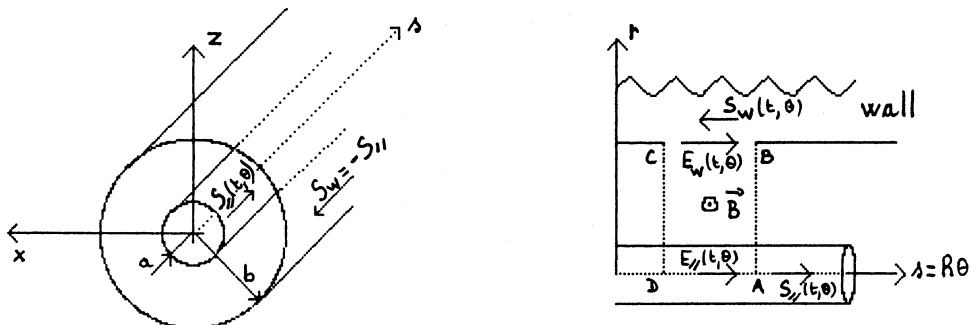


Fig. 5 Boundary conditions for an on-axis beam in a perfectly-conducting circular pipe

At time t and angular position θ in the machine, the local beam current is given by the signal $S_{\parallel}(t, \theta)$.

Let us assume that the beam is completely screened by the pipe wall. Then, there is no electromagnetic field outside the chamber. When applied to a 2π path enclosing the chamber cross section, Ampere's theorem leads to

$$\oint \vec{H} \cdot d\vec{l} = I_{total}(t, \theta) \quad (41)$$

where $I_{total}(t, \theta)$ is the total current through the path plane. Since we already have the beam current $S_{\parallel}(t, \theta)$ flowing downstream, it has to be exactly balanced by a return current or image current flowing upstream in the wall thickness.

$$S_w(t, \theta) = -S_{\parallel}(t, \theta) \quad (42)$$

For perfectly conducting walls, the electric field in the wall E_w that has to be associated with the image current S_w is null. Well below the pipe cut-off frequency, that stands in the GHz region

$$\omega_{\text{cut-off}} = \frac{c}{b} , \quad (43)$$

one can apply Faraday's law in the longitudinal cross section of the pipe, along a contour like ABCD (Fig. 5).

$$\oint \vec{E} \cdot d\vec{l} = - \frac{\partial}{\partial t} \int \vec{B} \cdot d\vec{s} . \quad (44)$$

The result is the standard longitudinal space charge field set up by the direct current $S_{||}(t, \theta)$.

In terms of wall current, this space charge field can be written

$$2\pi R E_{||, \text{s.c.}}(t, \theta) = \frac{-Z_0 q}{2\beta\gamma^2\omega_0} \frac{\partial}{\partial t} S_w(t, \theta) \quad (45)$$

$Z_0 = 377 \text{ ohm}$ is the space free impedance
 $q = 1 + 2 \ln(\frac{b}{a})$

Therefore, the space charge impedance is a negative inductance,

$$L_{\text{s.c.}} = - \frac{Z_0 q}{2\beta\gamma^2\omega_0} . \quad (46)$$

Large for low- β particles, it vanishes at ultrarelativistic energies. In the form of equation (40), in terms of signal, it can be written

$$2\pi R E_{||, \text{s.c.}}(t, \theta) = - \int_{\omega=-\infty}^{\omega=+\infty} \frac{Z_0 q \omega}{1 + 2\beta\gamma^2\omega_0} S_{||}(\omega, \theta) e^{j\omega t} d\omega . \quad (47)$$

For resistive walls, the electric field in the wall E_w is different from zero. Due to the skin effect impedance an additional electric field appears on beam axis.

$$2\pi R E_{||, \text{R.W.}}(t, \theta) = - \int_{\omega=-\infty}^{\omega=+\infty} Z_{||, \text{R.W.}}(\omega) S_{||}(\omega, \theta) e^{j\omega t} d\omega . \quad (48)$$

The resistive wall impedance is given by

$$Z_{||, \text{R.W.}}(\omega) = (1 + j) \frac{Z_0 \beta}{2b} \delta_o^* \left(\frac{\omega}{\omega_0} \right)^{\frac{1}{2}} \quad \delta_o^* = \sqrt{\frac{\epsilon_r}{\mu_0 \omega_0}} \quad (49)$$

where δ_0^* is the skin depth at revolution frequency.

ρ = resistivity $\sim 1.10^6 \Omega m$ for stainless steel, $\mu_0 = 4\pi \cdot 10^{-7}$.

In these two examples of fields the environment enters via its geometry (boundary conditions imposed at distance b) and via its electromagnetic properties (resistivity ρ in δ_0^* for instance). Obviously different machines have different wall geometries and different wall electromagnetic properties. Accordingly, the impedance varies from one machine to another.

Since the impedance is a key parameter that rules instability threshold current, many attempts have been made to measure, to understand and to minimize machine impedances.

The quantity of interest is not the longitudinal impedance itself but the impedance divided by the frequency $Z_{\parallel}(\omega)/\omega$ or even better, $Z_{\parallel}(p)/p$ the impedance divided by the harmonic number p of the revolution frequency $\omega = p\omega_0$. In a diagram with $Z_{\parallel}(p)/p$ along the vertical axis and ω running from $-\infty$ to $+\infty$ along the horizontal axis, a pure inductance $jL\omega$ is associated with a constant $I_m(Z_{\parallel}(p)/p) = L\omega_0$, a pure resistance R is represented by an hyperbola $R_e(Z_{\parallel}(p)/p) = R\omega_0/\omega$.

The main components of the impedance that can be found in a standard circular machine are listed hereunder and sketched in Fig. 6.

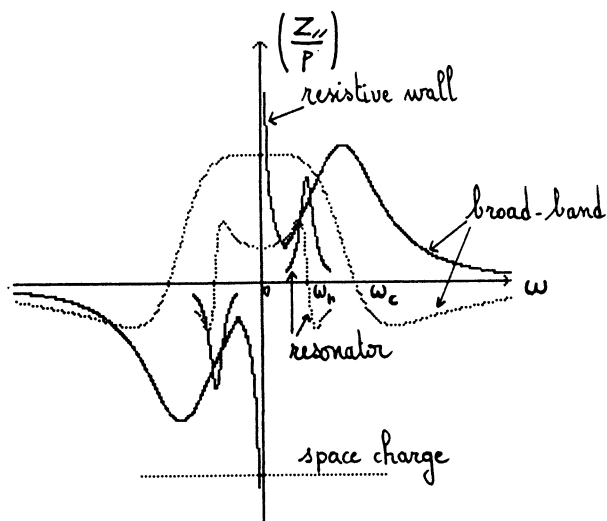


Fig. 6 Qualitative description of longitudinal impedance for various components (full line = real part, dotted line = imaginary part)

a) Resistive wall component

It is peaked at low frequency.

$$\frac{Z_{\parallel RW}}{P} = (1 + \frac{1}{f}) \frac{Z_0 \beta}{2b} \delta_0^* \frac{1}{\sqrt{p}} \quad (\text{thick wall assumption}) \quad (50)$$

We will see that longitudinal modes have no spectral amplitude at low frequencies. As a consequence, it acts very weakly on longitudinal motion and can be disregarded.

b) Narrow band resonators

One of them, at $\omega_r = h\omega_0$, is the necessary RF system that keeps the beam bunched. One can also find parasitic high Q resonators due to higher order modes in RF cavities for instance.

c) Broad band component (BB)

The averaged effect of numerous changes in vacuum chamber cross section (step changes, bellows, tanks, electrodes, etc) can be approximated by a low $Q \sim 1$ resonator with the resonance ω_r at pipe cut-off frequency (43).

The origin of the mechanism is the electromagnetic field created by the beam itself

$$Z_{\parallel B.B.}(\omega) = \frac{R_s}{1 + jQ\left(\frac{\omega}{\omega_r} - \frac{\omega_r}{\omega}\right)} \quad (51)$$

R_s is the shunt impedance in ohm
 Q the quality factor.

It acts like a pure inductance at low frequencies,

$$\frac{Z_{\parallel B.B.}(p)}{p} = j R_s \frac{\omega_0}{\omega_r} \quad (52)$$

like a pure resistance at resonance,

$$\frac{Z_{\parallel B.B.}(p)}{p} = R_s \frac{\omega_0}{\omega_r} \quad (53)$$

It acts like a capacitance at high frequencies,

$$\frac{Z_{\parallel B.B.}(p)}{p} = -j R_s \frac{\omega_r \omega_0}{\omega^2} \quad (54)$$

This broad band model is in quite good agreement with experimental results. For those machines carefully designed to lower the BB impedance, the peak value of $|Z_{\parallel}(p)/p|$ can be as low as a fraction of an ohm. It can reach 50 Ω when no care at all is taken.

d) Space charge component

$$\frac{Z_{\parallel s.c.}(p)}{p} = -j \frac{Z_0 \gamma}{2 \beta \gamma^2} \quad (55)$$

It can be very large for low- β particles.

$$\begin{aligned} &\sim 1.5 \text{ k}\Omega \text{ for } \beta = .3 \quad (50 \text{ MeV protons}) \\ &\sim 7 \text{ }\Omega \text{ for } \beta = .7 \quad (7 \text{ GeV protons}). \end{aligned}$$

The actual impedance seen by the beam is the sum of the components listed above.

2.5 Effect of the stationary distribution

In the first part of this section, we are still assuming a single bunch in the machine.

The effect of the electromagnetic field induced by the stationary distribution q_0 is included in the single particle differential equation of motion

$$\ddot{\tau} + \omega_{s0}^2 \tau = F_0 = \frac{n e}{P_{\parallel}} \left[\vec{E} + \vec{\beta}_c \wedge \vec{B} \right]_{\parallel} (t, \theta = \omega_0(t-\tau)) \quad (56)$$

$$\theta = \omega_0(t-\tau) \text{ when following the particle.}$$

The right hand side of equation (56) can be developed by using equations (40), (21), (23), (6) successively.

$$F_0 = \frac{2\pi I \omega_{s0}^2}{\omega_0 V_{R.F.} h \cos \psi_s} \sum_p Z_{\parallel}(p) \sigma_0(p) e^{j p \omega_0 \tau} \quad (57)$$

In the following, we will be concerned with small amplitudes. Therefore we can expand the exponential in series:

$$\ddot{\tau} + \omega_{s_0}^2 \tau = \frac{2\pi I \omega_{s_0}^2}{\omega_0 V_{RF} h \cos \varphi_s} \sum_p Z_{\parallel}(p) \sigma_o(p) \left\{ 1 + \int p \omega_0 \tau - \frac{p^2 \omega_0^2 \tau^2}{2} + \dots \right\}. \quad (58)$$

Let us analyze equation (58). In the absence of self-field, a linear motion has been assumed. The external RF voltage varies linearly with time during the bunch passing and all particles oscillate at the same frequency ω_{s_0} whatever their amplitude $\hat{\epsilon}$ is.

The stationary self field introduces :

- a zero order term that changes the synchronous phase,
- a first order term responsible of the incoherent frequency shift,
- non-linear terms which make the frequency shift amplitude dependent. Some synchrotron frequency spread appears.

2.5.1 Synchronous phase shift "higher-mode loss"

The constant term in equation (58) moves the stable fixed point

$$\Delta \varphi_s = h \omega_0 \Delta \tau = \frac{2\pi I}{V_{RF} \cos \varphi_s} \sum_p R_e(Z_{\parallel}(p)) \sigma_o(p). \quad (59)$$

Because of the power dissipated in the wall by the return current the beam loses energy. The synchronous phase is displaced so that this loss can be restored by the RF system.

Equation (59) can be used to probe the resistive part of the impedance.

We will see later on that this effect tends to lower the synchrotron frequency and contributes to bunch lengthening.

2.5.2 Incoherent frequency shift - Potential well distortion

When gathering first order terms of equation (58), we get

$$\omega_s^2 = \omega_{s_0}^2 \left(1 - \frac{2\pi I}{V_{RF} h \cos \varphi_s} \sum_p \int Z_{\parallel}(p) p \sigma_o(p) \right). \quad (60)$$

$p \sigma_o(p)$ is an odd function with respect to p , therefore resistance does not modify the synchrotron frequency.

When the bunch is long enough, $2\pi/\tau_L \ll \omega_{cut-off}$, the major part of the stationary spectrum stands in the low frequency region where space-charge impedance and broadband impedance are constant. Under these assumptions, equation (60) can be rewritten

$$\Delta = \frac{\omega_s^2 - \omega_{s_0}^2}{\omega_{s_0}^2} = - \frac{2\pi I}{V_{RF} h \cos \varphi_s} \left[\int \frac{Z_{\parallel}(p)}{p} \right]_{S.C. \atop B.B.} \sum_p p^2 \sigma_o(p). \quad (61)$$

For the bunch with parabolic amplitude (25) with the help of

$$\sum_{p=-\infty}^{p=\infty} J_z(p x) = \frac{2}{x}$$

we get

$$\Delta = \frac{\omega_s^2 - \omega_{s_0}^2}{\omega_{s_0}^2} = - \frac{16 I}{\pi^3 B^3 V_{RF} h \cos \varphi_s} \Re \frac{Z_{\parallel}(p)}{p} = \frac{V_T}{V_{RF}} - 1 . \quad (62)$$

Below the transition energy $\cos \varphi_s > 0$ the synchrotron frequency is reduced by space charge $\Re Z_{\parallel}(p)/p > 0$ and increased by the B.B. inductance $\Im Z_{\parallel}(p)/p < 0$. The reverse applies above transition. The same qualitative remarks are valid for any stationary distribution.

The change in RF slope corresponds to an effective voltage V_T given by

$$\frac{V_T}{V_{RF}} = \left(\frac{\omega_s}{\omega_{s_0}} \right)^2 . \quad (63)$$

If we consider a parabolic line density bunch (26) interacting with a constant $I_m(Z_{\parallel}(p)/p)$, then, without any approximation, equation (56) can be reduced to

$$\ddot{\tau} + \omega_{s_0}^2 \tau = \frac{3 I}{\pi^2 V_{RF} h \cos \varphi_s B^3} \Im Z_{\parallel}(p) \tau . \quad (64)$$

In this particular case, the focusing force is purely linear. The corresponding incoherent frequency shift is given by

$$\Delta = \frac{\omega_s^2 - \omega_{s_0}^2}{\omega_{s_0}^2} = \frac{3 I}{\pi^2 V_{RF} h \cos \varphi_s B^3} \Re \frac{Z_{\parallel}(p)}{p} \quad (65)$$

which is about two times less than (62).

In Fig. 7 the potential-well distortion corresponding to a long bunch interacting with a B.B. above transition is sketched.

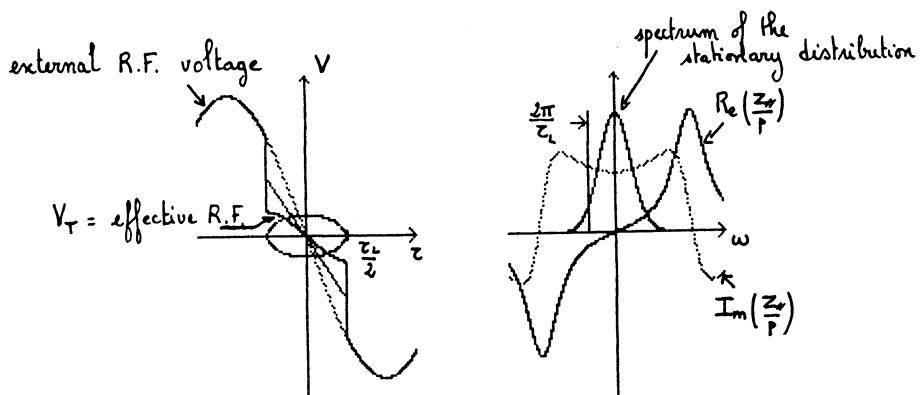


Fig. 7 Distortion of the RF wave form (left) due to the interaction with an inductive broad-band resonance (right)

2.5.3 Bunch lengthening

A direct consequence of the shifts of the synchronous phase and of the incoherent frequency is that the bunch length and momentum spread depend on intensity.

For electrons, the equilibrium momentum spread is imposed by radiation. Then,

$$\frac{B}{B_0} = \frac{\omega_{s0}}{\omega_s} \left(\frac{\cos \varphi_s}{\cos(\varphi_s + \Delta\varphi_s)} \right)^{\frac{1}{2}} \quad (66)$$

in which, B_0 is the bunching factor for zero intensity.

It is a transcendental equation since B appears in ω_s and in $\Delta\varphi_s$.

The synchronous phase shift lowers the incoherent synchrotron frequency. Above transition, with long bunches $2\pi/\tau_L \ll \omega_{cut-off}$ the inductance of the broad-band impedance has the same effect (with very short bunches, the stationary spectrum reaches the B B capacitance and this last contribution can be reversed).

In most cases the synchronous phase shift can be neglected. This allows us to rewrite equation (66) in the following form

$$\frac{B}{B_0} = \left(\frac{B}{B_0} \right)^3 + \Delta_0 \quad (67)$$

in which $\Delta_0 = ((\omega_s^2 - \omega_{s0}^2)/\omega_{s0}^2)$, is the normalized deviation of frequencies squared one would obtain with $B = B_0$ (nominal current associated with zero current bunch length).

For protons, we assume that the emittance is invariant. Therefore,

$$\left(\frac{B}{B_0} \right)^2 = \frac{\omega_{s0}}{\omega_s} \left(\frac{\cos \varphi_s}{\cos(\varphi_s + \Delta\varphi_s)} \right)^{\frac{1}{2}} \quad (68)$$

holds.

When comparing the electron and the proton case, $(B/B_0)^2$ replaces B/B_0 . Therefore the bunch is less affected by the self field of the stationary distribution.

If one neglects the synchronous phase shift again, equation (68) can be written

$$\left(\frac{B}{B_0} \right)^{-1} = \left(\frac{B}{B_0} \right)^3 + \Delta_0 . \quad (69)$$

For Δ_0 the same definition as in equation (67) has to be used.

Since the emittance is constant for protons, the momentum spread has to be readjusted.

In Fig. 8, the solutions of equations (67) and (69) are drawn.

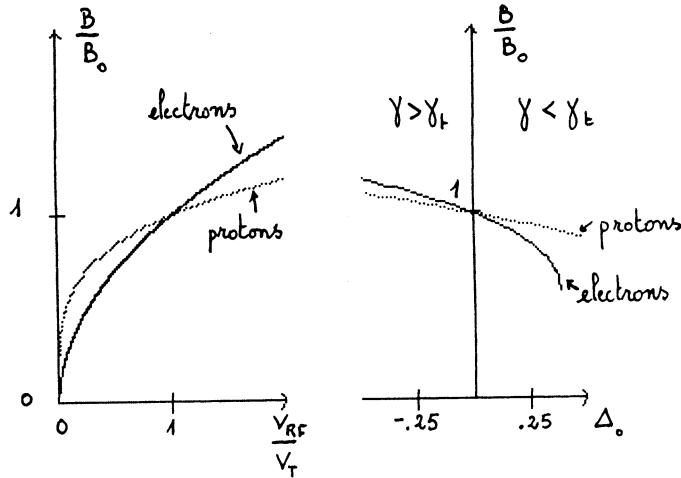


Fig. 8 Bunch lengthening as a function of current

2.5.4 Multibunch case

Now, we assume that the machine is operated in a multibunch mode. There are M identical bunches equally spaced corresponding to a total current MI . The spectrum is a line spectrum again, with the same form factor as the single bunch one. The spacing between lines is the bunch repetition frequency $M\omega_0$, that is to say M times larger than it was. On the other hand the spectrum amplitude is multiplied by M .

Equations (59) and (60) become

$$\Delta\psi_s = \frac{2\pi I}{V_{RF} h \omega \psi_s} M \sum_p R_e(Z_{||}(M_p)) \sigma_o(M_p) \quad (59)^*$$

$$\omega_s^2 = \omega_{so}^2 \left(1 - \frac{2\pi I}{V_{RF} h \omega \psi_s} M \sum_p \gamma Z_{||}(M_p) M_p \sigma_o(M_p) \right). \quad (60)^*$$

If the attenuation of the wake field between two successive bunches is weak, in other words, if the environment can memorize the passing of a bunch for a time larger than the bunch repetition period (abrupt change of the impedance within a frequency interval of the order of the repetition frequency), then, the results for the multibunch case (59)* and (60)* can be very different from the single bunch case (59) and (60).

On the other hand, if the interaction is a local one (delta function wake) such as space charge or inductive wall (constant $Z_{||}(p)/p$), bunches ignore each other, then, multibunch and single bunch cases lead to the same result. This is exactly the case for equations (61), (62) and (65).

This ends up our study of the electromagnetic field induced by the stationary distribution. For a given current, we have defined a new set of matched conditions that takes into account the external RF field and the self field of the stationary distribution. As long as parameters remain realistic, the stationary bunch is stable. In the rest of this lecture we will assume that all the above effects (synchronous phase shift, incoherent frequency shift, modified bunch length and momentum spread) have been taken into account.

Around the new fixed point, the linear equation of motion of the single particle is

$$\ddot{\tau} + \omega_s^2 \tau = 0 \quad (70)$$

and

$$\omega_s^2 = \frac{-\eta e \omega_0 V_T h \cos(\varphi_s + \Delta\varphi_s)}{2\pi R p_{\parallel}}. \quad (71)$$

2.6 Effect of the perturbation

Now, as suggested in section 2.3.2 we want to add a coherent perturbation that rotates at frequency ω_c in phase space and therefore induces some field at $p\omega_0 + \omega_c$.

2.6.1 Vlasov's equation

First we have to introduce the necessary equations to allow the evolution of the distribution to be followed.

The basic equation that rules the time evolution of the local density distribution is the collision-free Boltzmann's equation.

$$\frac{\partial \Psi}{\partial t} + \operatorname{div}(\Psi \vec{v}) = 0 \quad (72)$$

where

$$\vec{v} \begin{pmatrix} \dot{\tau} \\ \dot{\vec{z}} \end{pmatrix}.$$

It can be developed as follows

$$\frac{d\Psi}{dt} = -\Psi \operatorname{div} \vec{v}. \quad (73)$$

If one uses a set of canonical conjugate variables like (τ, \vec{z}) , then $\operatorname{div} \vec{v} = 0$ and an equivalent form of equation (70) is

$$\frac{d\Psi}{dt} = 0 = \frac{\partial \Psi}{\partial t} + \frac{\partial \Psi}{\partial \tau} \dot{\tau} + \frac{\partial \Psi}{\partial \vec{z}} \ddot{\vec{z}}. \quad (74)$$

In this form, it is called Vlasov's equation. It expresses that phase-space density does not vary with time when following the motion in canonical variables.

2.6.2 Equation of coherent motion

We consider a distribution that sums up a stationary distribution and a coherent perturbation $\Delta\Psi$ as described in equation (39).

$$\Psi(\psi_0, \vec{z}, t) = q_0(\vec{z}) + \sum_m q_m(\vec{z}) e^{-im\psi_0} e^{j(\omega_c - m\omega_s)t}. \quad (75)$$

We aim at finding out ω_c to study the stability via its imaginary part. We rewrite Vlasov's equation (74) with ψ_0 and \vec{z} as new variables.

$$0 = \frac{\partial \Delta\Psi}{\partial t} + \left(\frac{\partial q_0}{\partial \vec{z}} + \frac{\partial \Delta\Psi}{\partial \vec{z}} \right) \frac{d\vec{z}}{dt} + \frac{\partial \Delta\Psi}{\partial \psi_0} \frac{d\psi_0}{dt} \quad (76)$$

$\frac{\partial \Delta \Psi}{\partial t} \cdot \frac{d\psi}{dt}$ and $\frac{\partial \Delta \Psi}{\partial \hat{z}} \cdot \frac{d\hat{z}}{dt}$ are dropped since they represent second order terms with respect to the perturbation.

$$\int e^{j\omega_c t} \sum_m (\omega_c - m\omega_s) q_m(\hat{z}) e^{-j\hat{m}\psi} = - \frac{\partial q_0}{\partial \hat{z}} \frac{d\hat{z}}{dt} \quad (77)$$

$\psi = \omega_s t + \psi_0$ will be used to make the writing easier.

In the right-hand side of the linearized Vlasov's equation (77), we have to express the product

$$\frac{\partial q_0}{\partial \hat{z}} \frac{d\hat{z}}{dt} .$$

The stationary distribution comes in via its derivative with respect to \hat{z} . As pointed out before in section 2.3.1, distributions like the water bag distribution (28) with infinite $\frac{\partial q_0}{\partial \hat{z}}$ must be avoided.

The expression of $d\hat{z}/dt$ can be drawn from a single particle equation of motion.

$$\ddot{z} + \omega_s^2 z = F_c = \frac{qe}{p_{\parallel}} [\vec{E} + \vec{\beta}_c \wedge \vec{B}]_{\parallel} (t, \theta = \omega_0(t-z)) \quad (78)$$

$$\frac{d\hat{z}}{dt} = \frac{1}{dk} \left(\dot{z}^2 + \frac{\dot{z}^2}{\omega_s^2} \right)^{1/2} = - \frac{F_c}{\omega_s} \sin \psi \quad (79)$$

F_c is the coherent electromagnetic "force". Let us recall that the stationary distribution effect has been already taken into account (70) and (71).

By means of equations (40), (31), (32) and (71), F_c can be written :

$$F_c = \frac{2\pi I \omega_s^2 e^{j\omega_c t}}{\omega_0 V_T h \cos(\varphi_s + \Delta\varphi_s)} \sum_P \sum_{\parallel}(P) e^{jP\omega_0 t} \sum_k \sigma_k(P) . \quad (80)$$

It is interesting to notice that F_c does not depend on \dot{z} , therefore z and \dot{z} are canonical conjugate variables.

Now, we expand the product $\sin \psi e^{jP\omega_0 t}$ in series

$$\sin \psi e^{jP\omega_0 t} = \sum_r \int_r e^{-jr\psi} \frac{r}{P\omega_0} J_r(P\omega_0 \hat{z}) . \quad (81)$$

Equation (12) and

$$J_{r+1}(x) + J_{r-1}(x) = \frac{2r}{x} J_r(x) \quad (82)$$

have been used.

Finally we get

$$\hat{\tau} \frac{\partial q_0}{\partial \hat{\tau}} \frac{d\hat{\tau}}{dt} = - \frac{2\pi I_m \omega_s e^{j\omega_c t}}{\omega_0^2 V_T h \cos(\psi_s + \Delta\psi_s)} \frac{\partial q_0}{\partial \hat{\tau}} \sum_p \frac{Z_{rr}(p)}{p} \int e^{-j\omega_p t} J_r(p\omega_0 \hat{\tau}) \sum_k \sigma_k(p). \quad (83)$$

We gather both sides of equation (77) and notice that it splits into an infinite number of equations, one for each m . As a matter of fact, on an average, the component q_m of the perturbation is driven by the term $r=m$ essentially.

The final form of the equation of coherent motion of a single bunch is

$$\int (\omega_c - m\omega_s) \int^{-m\hat{\tau}} q_m = \frac{2\pi I_m \omega_s}{\omega_0^2 V_T h \cos(\psi_s + \Delta\psi_s)} \frac{\partial q_0}{\partial \hat{\tau}} \sum_p \frac{Z_{rr}(p)}{p} J_m(p\omega_0 \hat{\tau}) \sigma(p) \quad (84)$$

$\sigma(p)$ is the resultant spectrum amplitude at frequency $p\omega_0 + \omega_c$.

$$\sigma(p) = \sum_m \sigma_m(p) . \quad (85)$$

2.6.3 Coherent modes of oscillation

Because there are two degrees of freedom $(\psi_0, \hat{\tau})$, the general solution of equation (84) is a twofold infinity of coherent modes of oscillation. We will use the subscripts m and q ($-\infty < m, q < \infty$) to label these modes.

Each of them is characterized by

- a coherent frequency ω_{cmq} . Its imaginary part will tell us whether this mode is stable or unstable

- a particular perturbation $\Delta\Psi$. That is to say a twofold infinity of functions $g_{mq}(\hat{\tau})$, the sum of which gives the detailed density pattern that rotates in phase space at frequency ω_c .

- a spectrum $\sigma(p)$ which is obviously peaked in the frequency region where this mode is driven by the impedance. At low intensity the self force responsible for the frequency shift is small when compared to the external force responsible for the synchrotron frequency. The coherent frequencies of the infinity of modes with the same m value cluster near the unperturbed frequency $m\omega_s$. Therefore it is logical to study each family m separately and to ignore the coupling between different m .

When equation (84) is restricted to a single value of m ,

$$\int (\omega_{cmq} - m\omega_s) \int^{-m\hat{\tau}} g_{mq} = \frac{2\pi I_m \omega_s}{\omega_0^2 V_T h \cos(\psi_s + \Delta\psi_s)} \frac{\partial q_0}{\partial \hat{\tau}} \sum_p \frac{Z_{rr}(p)}{p} J_m(p\omega_0 \hat{\tau}) \sigma_{mq}(p) \quad (86)$$

there are several methods to get the solution.

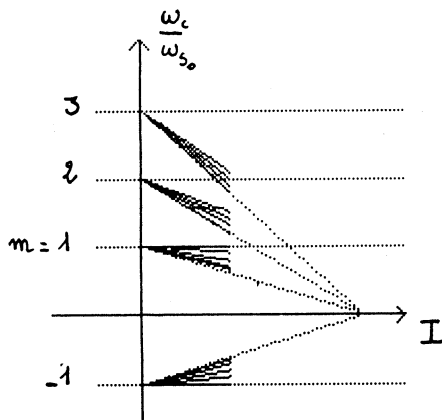


Fig. 9 Schematic representation of coherent-mode frequencies versus current

2.6.4 Sacherer's approach

The functions $g_{mq}(\hat{z})$ are solutions of Sacherer's integral equation.

$$(\omega_{cmq} - m\omega_s) g_{mq}(\hat{z}) + \frac{1}{\hat{z}} \frac{\partial g_0}{\partial \hat{z}} \int_0^\infty G_m(\hat{z}, \hat{z}') g_{mq}(\hat{z}') \hat{z}' d\hat{z}' = 0 . \quad (87)$$

The definition of σ_{mq} (32) has been used.
 $G_m(\hat{z}, \hat{z}')$ is the synthetic kernel.

$$G_m(\hat{z}, \hat{z}') = \frac{2\pi I m \omega_s}{\omega_0^2 V_T h \cos(\phi_s + \Delta\phi_s)} \sum_p \int \frac{Z_p(p)}{p} J_m(p\omega_0 \hat{z}) J_m(p\omega_0 \hat{z}') . \quad (88)$$

In search of solutions g_{mq} , let us study the properties of these functions.
We define an adjoint function

$$g_{ml}^+ = \frac{g_{ml}}{\frac{1}{\hat{z}} \frac{\partial g_0}{\partial \hat{z}}} \quad (89)$$

that satisfies

$$(\omega_{cmq} - m\omega_s) g_{ml}^+ + \int_0^\infty G_m(\hat{z}, \hat{z}') g_{ml}(\hat{z}') \hat{z}' d\hat{z}' = 0 . \quad (90)$$

Then we define the scalar product of two solutions g_{ml} and g_{mq} as follows

$$\langle g_{ml}, g_{mq} \rangle = \langle g_{mq}, g_{ml} \rangle = \int_0^\infty g_{mq}(\hat{z}) g_{ml}^+(\hat{z}) \hat{z} d\hat{z} \quad (91)$$

and we use equations (10) and (12) to express it:

$$(\omega_{cmq} - m\omega_s) \langle g_{ml}, g_{mq} \rangle = (\omega_{cmq} - m\omega_s) \langle g_{mq}, g_{ml} \rangle \\ = \int_{\hat{z}} \int_{\hat{z}'} G_m(\hat{z}, \hat{z}') g_{ml}(\hat{z}) g_{mq}(\hat{z}') \hat{z} \hat{z}' d\hat{z} d\hat{z}' = \frac{2\pi I m\omega_s}{\omega_0^2 V_T h \cos(\varphi_s + \Delta\varphi_s)} \sum_p \left(\int \frac{Z_l(p)}{p} \sigma_{mq}(p) \sigma_{mp}(p) \right). \quad (92)$$

We can conclude that :

- If $q \neq l$, the scalar product has to be null. Therefore, the solutions g_{mq} are orthogonal according to equation (91). This is the only information we have in order to get the solutions. A priori, these solutions which depend on g_0 via $\frac{1}{2} \frac{\partial g_0}{\partial z}$ are not necessarily expressible in terms of functions that exist in the standard library of functions.

- If the g_{mq} were known exactly, then, with $q = l$ in equation (92) one could get the coherent frequencies ω_{cmq} .

$$\omega_{cmq} = m\omega_s \left(1 + \frac{2\pi I}{\omega_0^2 V_T h \cos(\varphi_s + \Delta\varphi_s)} \left(\int \frac{g_{mq}^2}{\frac{1}{2} \frac{\partial g_0}{\partial z}} \hat{z} d\hat{z} \right) \sum_p \left(\int \frac{Z_l(p)}{p} \sigma_{mq}^2(p) \right) \right). \quad (93)$$

Furthermore, for a local interaction like space charge or inductive walls (constant $Z_l(p)/p$) $Z_l(p)/p$ can be removed out of the summation over p values. The kernel is a Dirac function and the spectra σ_{mq} are self orthogonal.

This last property allowed F. Sacherer to find out a simple exact solution with Jacobi and Legendre polynomials $P_m^{(\alpha, \beta)}$ and P_m . It is valid for a constant $Z_l(p)/p$ and corresponds to the bunch with parabolic line density (26).

$$\omega_{cmq} = m\omega_s \left(1 + \frac{2\pi I}{\omega_0^2 V_T h \cos(\varphi_s + \Delta\varphi_s)} \left(\int \frac{Z_l(p)}{p} C_{mq} \right) \right) \quad (94)$$

$$g_{mq}(\hat{z}) = \int_0^{2\pi} e^{iq\theta} P_m\left(\frac{i\hat{z}}{\tau_L} \cos\theta\right) d\theta \quad (95)$$

$$\Delta \lambda_{mq}(\tau) = P_m\left(\frac{i\tau}{\tau_L}\right). \quad (96)$$

2.6.5 G. Besnier expansion in orthogonal polynomials

We assume there exists a complete set of normalized functions $f_u(\hat{z})$ which fulfil the orthogonality relation (90).

$$\langle f_u(\hat{z}), f_v(\hat{z}) \rangle = \begin{cases} 0 & u \neq v \\ 1 & u = v \end{cases}. \quad (97)$$

We expand the solutions $g_{mq}(\hat{\tau})$ and the kernel $G_m(\hat{\tau}, \hat{\tau}')$ in terms of the f_u 's.

$$g_{mq}(\hat{\tau}) = \sum_{u=0}^{+\infty} a_u f_u(\hat{\tau}) \quad (98)$$

$$G_m(\hat{\tau}, \hat{\tau}') = \sum_{u,v} M_{uv}^m f_u^+(\hat{\tau}) f_v^+(\hat{\tau}') \quad . \quad (99)$$

Applying the orthogonality condition (97) several times we get an infinite system of linear equations.

$$(\omega_{cmq} - m\omega_s) a_u + \sum_v M_{uv}^m a_v = 0 \quad (100)$$

M_{uv}^m is the interaction matrix.

$$M_{uv}^m = \frac{2\pi I m \omega_s}{\omega_0^2 V_T h \cos(\varphi_s + \Delta\varphi_s)} (-1)^m \sum_p \sigma_{mf_u}(p) \sigma_{mf_v}(p) \left(\int \frac{Z_u(p)}{p} \right) \quad (101)$$

with

$$\sigma_{mf_u}(p) = \int^{-m} \int_0^\infty J_m(p\omega_0 \hat{\tau}) f_u(\hat{\tau}) \hat{\tau} d\hat{\tau} \quad .$$

Numerical solutions of the truncated equation (100) yield eigenvalues $\omega_{cmq} - m\omega_s$ and the eigenvectors a_u which allow to express g_{mq} (equation 98).

For the bunch with parabolic line density orthogonal functions with the required weight-function and a range which extends from 0 to $\tau_i/2$ can be obtained from the Jacobi polynomials. Laguerre polynomials can be used for a gaussian bunch.

2.6.6 J.L. Laclare's eigenvalue problem

We simply multiply both sides of equation (86) by $J_m(l\omega_0 \hat{\tau})$ and integrate over $\hat{\tau}$ values to get

$$(\omega_{cmq} - m\omega_s) \sigma_{mq}(l) = \sum_p K_{lp}^m \sigma_{mq}(p) \quad (102)$$

$$K_{lp}^m = - \frac{2\pi I m \omega_s \left(\int \frac{Z_u(p)}{p} \right)}{\omega_0^2 V_T h \cos(\varphi_s + \Delta\varphi_s)} \int_0^\infty \frac{\partial g_0}{\partial \hat{\tau}} J_m(p\omega_0 \hat{\tau}) J_m(l\omega_0 \hat{\tau}) d\hat{\tau} \quad . \quad (103)$$

For q running from $-\infty$ to $+\infty$,

$\omega_{cmq} - m\omega_s$ is the q^{th} eigenvalue
 $\sigma_{mq}(p)$ the q^{th} eigenvector

of the infinite matrix K_{lp}^m the elements of which are defined by equation (103) (one column and one row per frequency line). For numerical reasons, the matrix needs be truncated. It explores a finite frequency domain (smooth impedances over a large frequency range,

small details over a reduced frequency range). For a given problem its dimension have to be larger when compared to those of Besnier's matrix. On the other hand each coefficient is easier and faster to compute. As a matter of fact Besnier's coefficients are given by slowly converging series.

2.6.7 J. Wang and C. Pellegrini approach

This last method is based essentially on the same analysis as other's but the authors do not define the mode number m in their perturbation.

It has been developed to explain fast blow up of the beam in a time interval that could be less than the synchrotron period.

2.7 Low intensity coherent modes of oscillation

We are assuming a low intensity bunched beam which interacts with the different components of a standard circular impedance 2.4. The modes of oscillation are solutions of equation (102).

2.7.1 Local interaction space charge or inductive walls

Because $\int \frac{Z_{\parallel}(p)}{p}$ is constant and real,

$$\int \frac{Z_{\parallel}(p)}{p} = \frac{Z_0 q}{2\beta^2} - L\omega_s \quad \omega \leq \omega_c \quad (104)$$

the matrix is real and symmetrical. The eigenvectors σ are orthogonal, the eigenvalues $\omega_{cmq} - m\omega_s$ are real. There is no instability. Once started, a pure eigenmode rotates indefinitely at coherent frequency in phase space.

Figure 10 illustrates the results for the bunch with parabolic amplitude (25).

The coherent frequency shifts can be written

$$\Delta\omega_{cmq} = \omega_{cmq} - m\omega_s = \frac{4I_m\omega_s}{\pi^2 B^3 V_T h \cos(\varphi_s + \Delta\varphi_s)} C_{mq} \left(\int \frac{Z_{\parallel}(p)}{p} \right) . \quad (105)$$

The largest C_{mq} values are listed in Fig. 10 in a decreasing order for the lowest values of m . Given m , the largest C_{mq} takes the subscript $q=m$, the next one $q=m+2$, ..., $q=m+2k$, ... $0 \leq k < \infty$.

The spectrum of mode $m q$ is peaked at $\omega \sim (q+1)\pi/\tau_L$ and extends $\pm 2\pi/\tau_L$ rad/sec.

Often, only the most coherent modes, with $q=m$ are referred to $m=1$ and $q=1$ dipole $m=2$ and $q=2$ quadrupole $m=3$ and $q=3$ sextupole etc... It should be noted that two modes with same q are peaked at the same frequency (same line density). They also have roughly the same C_{mq} and accordingly the same sensitivity in the same frequency range. Nevertheless they correspond to entirely different density patterns in phase space (compare g_{13}, S_{13} and g_{33}, S_{33} for instance).

Provided the bunch is long enough and the q value is not too large so that the main part of the mode spectrum stands well below the cutoff frequency, equation (105) gives a good approximation of space charge and broad band inductance effects.

In order to understand the physical meaning of the coherent frequency shift let us take the dipole mode $m=q=1$ and let us compare the coherent frequency ω_{c11} with the zero intensity incoherent frequency ω_{s0} .

The quantity $\omega_{c11} - \omega_{s0}$ is obtained

$$\omega_{c11} - \omega_{s0} = \omega_{c11} - \omega_s + \omega_s - \omega_{s0} = \Delta\omega_{c11} + \Delta\omega_i$$

by adding the coherent (105) and the incoherent (62) shifts.

$$\omega_{c11} - \omega_{s0} = \frac{4I\omega_s}{\pi^2 B^3 V_T h \cos(\varphi_s + \Delta\varphi_s)} \left(\int \frac{Z_{\parallel}(p)}{p} \right) \left(C_{11} - \frac{2}{\pi} \right) . \quad (106)$$

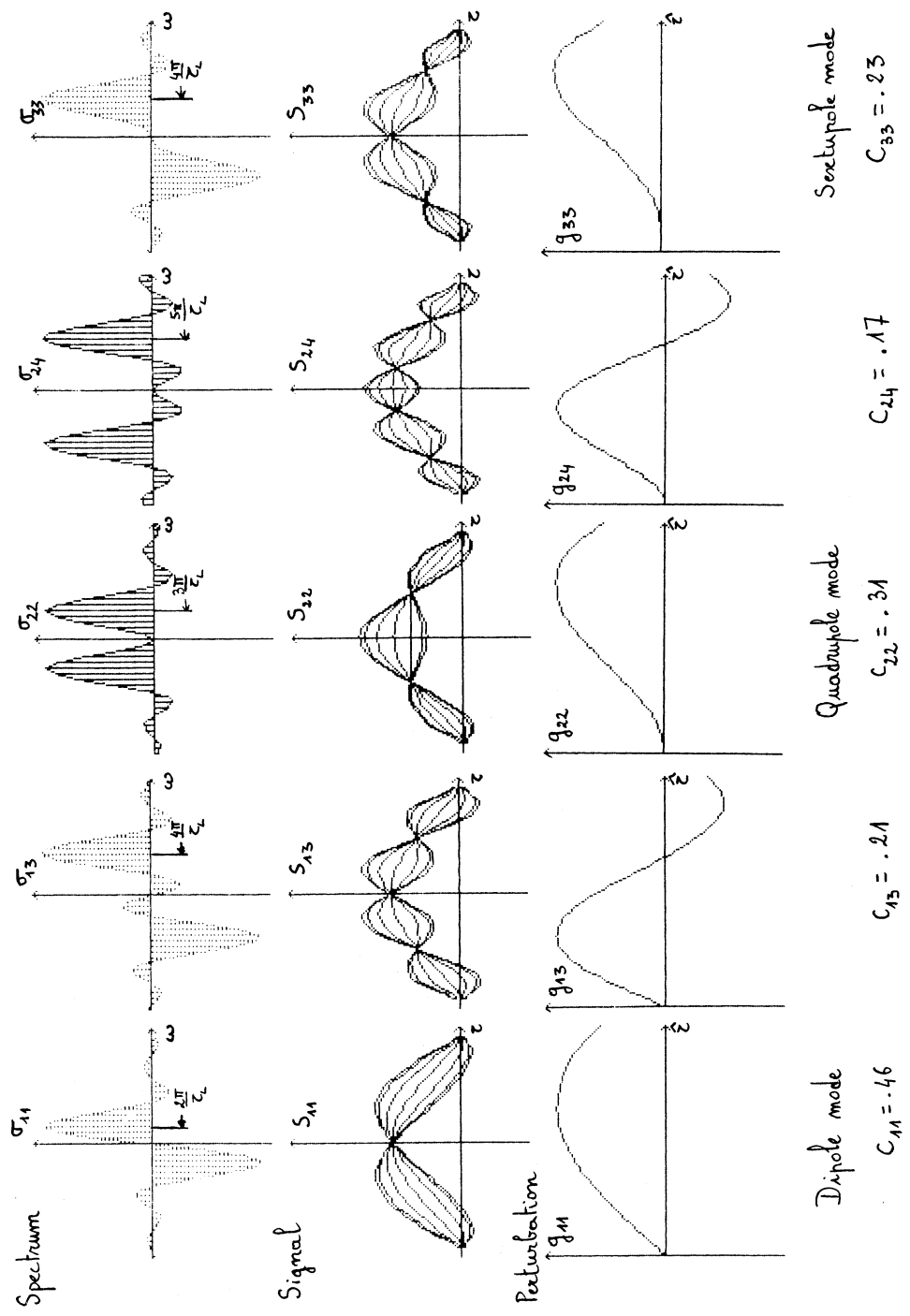


Fig. 10 Coherent modes of oscillation for a parabolic bunch distribution in an inductive impedance

Therefore, as far as frequencies are concerned, coherent and incoherent effects subtract. The frequency of the dipole mode is pushed back towards ω_{so} . We would obtain $\omega_{cm} = \omega_{so}$ exactly if a bunch with parabolic line density were assumed.

Depending on the stationary distribution, the dipole mode corresponds more or less to an off-centered rigid motion of the bunch in phase space. For a pure rigid motion (Fig. 11), the potential well deformation (change of focusing) induced by the stationary distribution is a pure quadrupole attached to the bunch center of mass position. Therefore, the bunch center of mass does not see any electric field change. It keeps oscillating in the external RF guide field and oscillates at frequency ω_{so} .

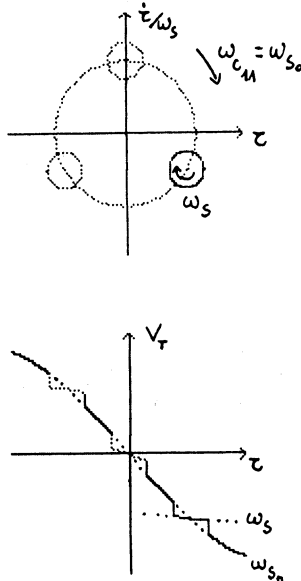


Fig. 11 Rigid dipole motion in phase space and induced potential inside the bunch

The coherent frequency shifts $\Delta\omega_{cmq}$ get smaller and smaller with increasing values of m and q . Nevertheless the overall tendency is to push back the coherent frequency towards $m\omega_{so}$ (see Fig. 9).

2.7.2 Parastitic high Q resonators - Coupled bunch modes

Let us imagine a very narrow band object, so narrow that the coherent motion is driven by a single line at $p\omega_0 + \omega_c$. Going back to the matrix equation (102), (103) valid at low intensity for a single value of m , we can write

$$(\omega_{cm} - m\omega_s) \sigma_m(l) = K_{lp}^m \sigma_m(p) \quad (107)$$

The sum over p has disappeared. A single coherent mode of m type is solution of equation (107).

- coherent frequency

$$\omega_{cm} = m\omega_s \left(1 - \frac{2\pi I}{\omega_0^2 V_T h \cos(\varphi_s + \Delta\varphi_s)} \int \frac{Z_r(p)}{p} \int_0^\infty \frac{\partial q_0}{\partial \hat{z}} J_m^2(p\omega_0 \hat{z}) d\hat{z} \right) \quad (108)$$

- spectrum

$$\sigma_m(p) = 1 \quad (109)$$

$$\sigma_m(l) = \frac{\int_0^\infty \frac{\partial g_0}{\partial \hat{z}} J_m(l\omega_0 \hat{z}) J_m(p\omega_0 \hat{z}) d\hat{z}}{\int_0^\infty \frac{\partial g_0}{\partial \hat{z}} J_m^2(p\omega_0 \hat{z}) d\hat{z}} \quad (110)$$

- perturbation (see equation (39))

$$\hat{\tau} g_m(\hat{z}) \propto \frac{\partial g_0}{\partial \hat{z}} J_m(p\omega_0 \hat{z}) . \quad (111)$$

Let us examine the stability of such a system

$$I_m(\omega_c) \propto \frac{-m}{V_T \cos(\varphi_s + \Delta\varphi_s)} R_e \left(\frac{Z_r(p)}{p} \right) \int_0^\infty \frac{\partial g_0}{\partial \hat{z}} J_m^2(p\omega_0 \hat{z}) d\hat{z} . \quad (112)$$

A resistance is needed in order to get an imaginary frequency shift.

A priori, g_0 is a monotonic decreasing function null at bunch edge $\hat{z} = \tau_L/2$. Therefore the integral in (112) is negative.

On the other hand, $V_T \cos(\varphi_s + \Delta\varphi_s)$ is negative above transition and $R_e(Z_r(p)/p)$ is positive at positive frequencies.

The conclusion is the following. Above transition, upper (lower) synchrotron sidebands as seen by a spectrum analyser have a destabilizing (stabilizing) effect, with the opposite below transition.

This result can be qualitatively explained by means of Fig. 12.

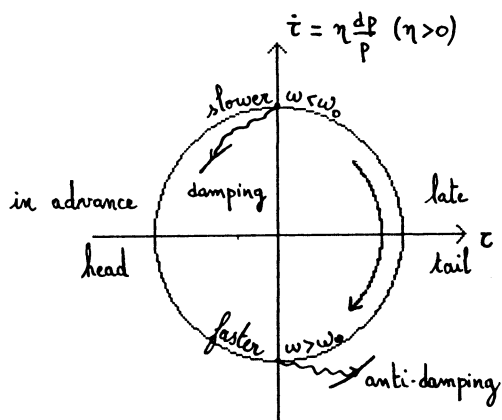


Fig. 12 Qualitative description of the synchrotron motion in phase-space

Above transition ($\eta > 0$), a positive $d\varphi/\varphi$ is associated with a positive $\dot{\varphi}$ and a lower revolution frequency. Therefore, the upper part of the phase-space diagram coincides with contribution to the lower sidebands of the spectrum.

If we assume a rigid dipole mode oscillation, when the bunch center of mass is at noon in phase space, it loses energy by interacting with the resistance at lower sideband frequencies. It spirals towards the synchronous particle, the coherent amplitude is damped.

On the other hand, the resistance associated with upper sidebands will have a destabilizing effect in the lower part of phase space diagram.

Up to now, a single bunch has been assumed and by means of a coherent perturbation $\Delta \Psi$ (see equation (39)), particles within this bunch have been arranged in order to produce a coherent signal at $p\omega_0 + \omega_s$.

If M equidistant bunches are present in the ring, one can go further and coherently arrange particles within successive bunches to obtain a coupled bunch coherent motion.

With the index n running from 0 to $M-1$, coupled bunch mode number n will correspond to a phase shift of $n \cdot \pi/M$ between the coherent perturbations of two successive bunches.

The Fourier component of the signal is M times larger but only every M^h line occurs.

With the above convention, the spectrum of coupled bunch mode is at frequencies

$$\omega_n = (n + pM) \omega_0 + m \omega_s . \quad (113)$$

The equations of coherent coupled bunch motion are essentially the same as the equations of coherent single bunch motion (84), (86), (102), (103) except that, I , current in one bunch becomes MI current in M bunches.

Indeed, the summation over the spectrum is restricted to the coupled bunch mode spectrum.

B remains the bunching factor of the single bunch (24).

An example is given in Fig. 13. We are considering $M=4$ bunches performing a coherent coupled bunch dipole mode. The four possibilities of coupling the bunches in phase space are shown in the upper part of the figure. In the lower part, the line spectrum is drawn as seen by a spectrum analyser.

The spacing between upper (destabilizing above transition) and lower (stabilizing) sidebands is minimum ($\Delta\omega = 2\omega_c$) for coupled bunch mode $n=0$ and $n=M/2$. It is maximum ($\Delta\omega = \frac{M}{2}\omega_0 + 2\omega_c$) for $n=\frac{M}{4}$ and $n=\frac{3M}{4}$.

As a consequence, modes $n=M/4$ and $n=3M/4$ are very sensitive to narrow band resonators. When mode n is damped (antidamped) the complementary mode $M-n$ is antidamped (damped). The maximum frequency shift is obtained when the resonator frequency coincides with one of the frequency lines in the coupled bunch mode signal $\omega_r = \omega_n$.

Provided the spacing between two adjacent lines of the spectrum is larger than the resonator bandwidth $\delta\omega$,

$$\delta\omega = \omega_r / 2Q \quad (114)$$

a single line drives the mode. Equation (108) applies. It can be adapted to the bunch with parabolic amplitude (25).

$$\frac{\omega_c - m\omega_s}{m\omega_s} = \frac{4MI}{(m+1)\pi^2 B^2 V_r h \cos(\varphi_s + \Delta\varphi_s)} \sqrt{\frac{R_s \omega_0}{\omega_r}} F_m(\omega_r, \frac{\omega_c}{2}) \quad (115)$$

$$F_m(x) = \frac{2(|m|+1)}{x^2} \int_0^x J_m^2(u) u du \quad (116)$$

R_s is the shunt impedance (see equation (51) for instance).

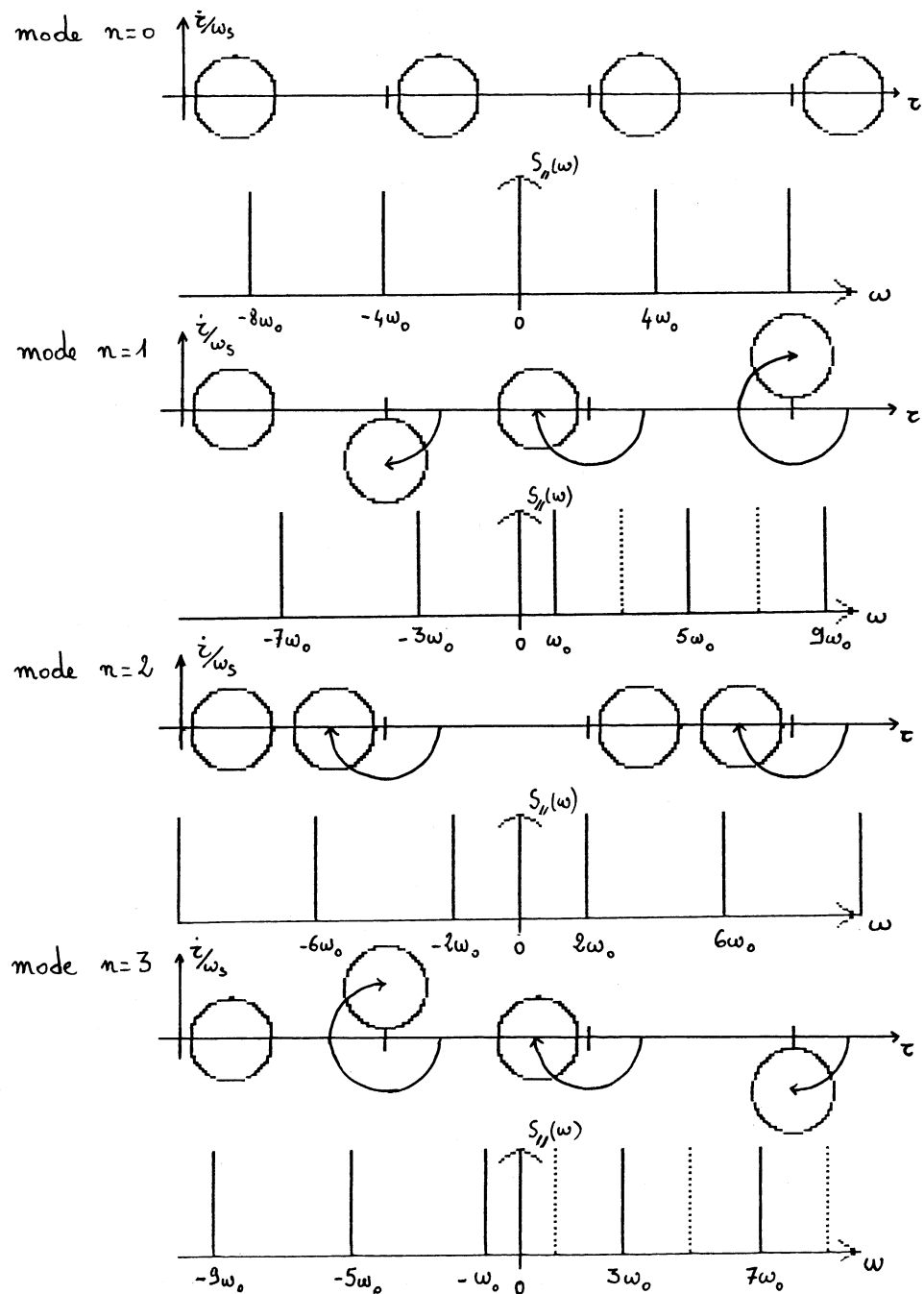


Fig. 13 Coherent coupled-bunch modes of four bunches

The form factor F_m is plotted in Fig. 14.

For large bandwidths (broad band impedance for instance), more than one line must be included in the frequency shift calculation. Cancellation occurs between upper and lower sidebands. The frequency shift is reduced by the factor D shown in Fig. 15.

$$D = \frac{\alpha}{\sinh \alpha} \quad (117)$$

The quantity

$$\alpha = \frac{\omega_r}{2Q} \cdot \frac{2\pi}{\omega_0} \cdot \frac{1}{M} \quad (118)$$

is the attenuation of the wake between successive bunches. There is no instability for wakefields that decay appreciably before the next bunch arrives.

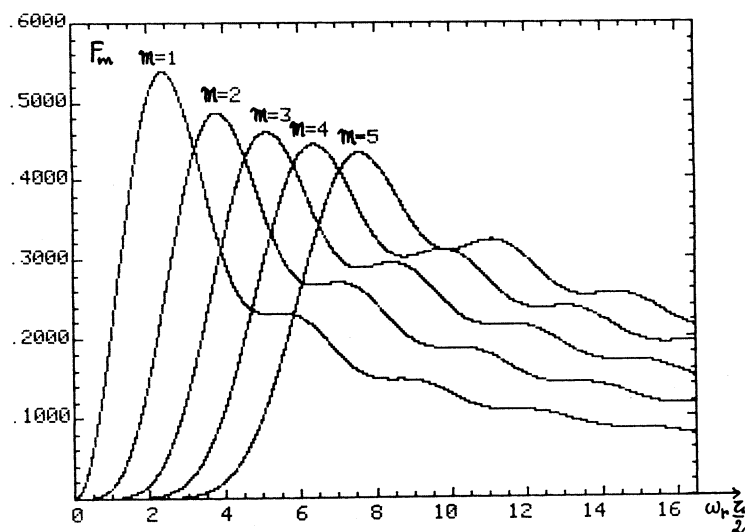


Fig. 14 Form factors F_m for different modes m of longitudinal bunch oscillation

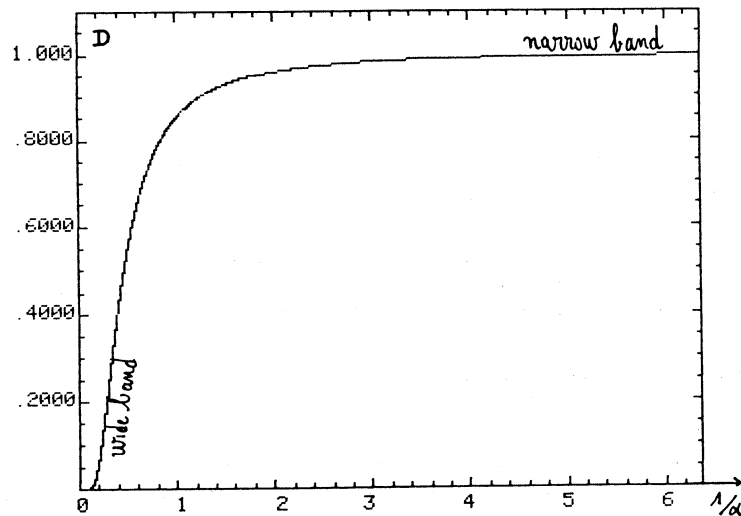


Fig. 15 Attenuation factor for the frequency shift in the case of a resonator impedance

Coupled bunch coherent instability is very harmful and difficult to fight.

Non-linearities can Landau damp the mechanism. When assuming some spread in incoherent synchrotron frequency, the threshold current is defined by

$$\Delta\omega_c \leq \frac{\sqrt{m}}{4} \Delta\omega_{\text{spread}} . \quad (119)$$

In the above expression, $\Delta\omega_{\text{spread}}$ is the full spread in ω between center and edge of the bunch due to non-linear synchrotron forces.

A spread in incoherent frequencies of individual bunches can also help in decoupling. This spread can be provided by a low frequency RF system. It can come from a spread in bunch population as well, in which case the required r.m.s spread is given by

$$\left\langle \frac{\delta I}{I} \right\rangle_{\text{r.m.s}} > \frac{I_m(\Delta\omega_c)}{R_e(\Delta\omega_c)} . \quad (120)$$

Indeed, one can imagine a feed back system to damp this type of instability. Nevertheless, the number of coupled bunch modes and consequently the number of bunches has to be limited in order to keep the feed back system bandwidth down.

2.7.3 RF cavity - Robinson's effect

For a single bunch or two bunches, upper and lower sidebands belong to the same coupled bunch mode and therefore tend to cancel unless the impedance is very narrow band as in an RF cavity.

The RF is tuned to ω_{RF} very close to $\hbar\omega_0$. Given m , the imaginary part of the frequency shift can be obtained by adding the effect of the upper and lower coherent sidebands (at $\hbar\omega_0 + m\omega_s$ and $\hbar\omega_0 - m\omega_s$ when the real part of the frequency shift is neglected $R_e(\omega_c - m\omega_s) \ll \omega_s$).

Let $R(\omega)$ be the resistance at frequency ω , we apply equation (108) and find

$$I_m(\omega_c) = -\frac{2\pi I_m m\omega_s}{\omega_0^2 V_r h^2 \cos(\psi_s + \Delta\psi_s)} [R(\hbar\omega_0 + m\omega_s) - R(\hbar\omega_0 - m\omega_s)] \int_0^\infty \frac{d\zeta}{\zeta} J_m^2(\hbar\omega_0 \zeta) d\zeta . \quad (121)$$

It is important to notice that the result is different from zero essentially because $R_e(Z_r(p)/p)$ is evaluated at $\hbar\omega_0 + m\omega_s$ while $R_e(Z_r(-p)/-p)$ is evaluated at $\hbar\omega_0 - m\omega_s$.

Trouble is avoided in this case by tuning the cavity to overlap the stable sideband according to Robinson's criterion.

2.7.4 Resistive wall impedance

The resistive wall impedance is peaked at low frequencies where the spectral amplitude of longitudinal modes is very weak. In most cases this effect can be disregarded.

2.7.5 Conclusions about coherent instabilities at low intensity

The theory that has been developed here above is in perfect agreement with observations.

The frequency shift formula looks reliable. It has been tested on several low order modes with space charge dominated beams as well as ultrarelativistic beams in inductive walls. Nowadays, it is often used to measure the reactive part of the impedance at low frequencies.

The predicted bunch shape oscillations (up to sextupole mode) are observable in many machines. In Fig. 16 top, photographs of a dipole mode (left) and of a quadrupole mode (right) are presented.

Coupled bunch modes are frequently observed in machines operated in multibunch mode. In Fig. 16 bottom, one can observe coupled bunch mode $n=1$ with three bunches in SATURNE (Saclay).

Lastly, the theory gives a good picture of Robinson's instability.

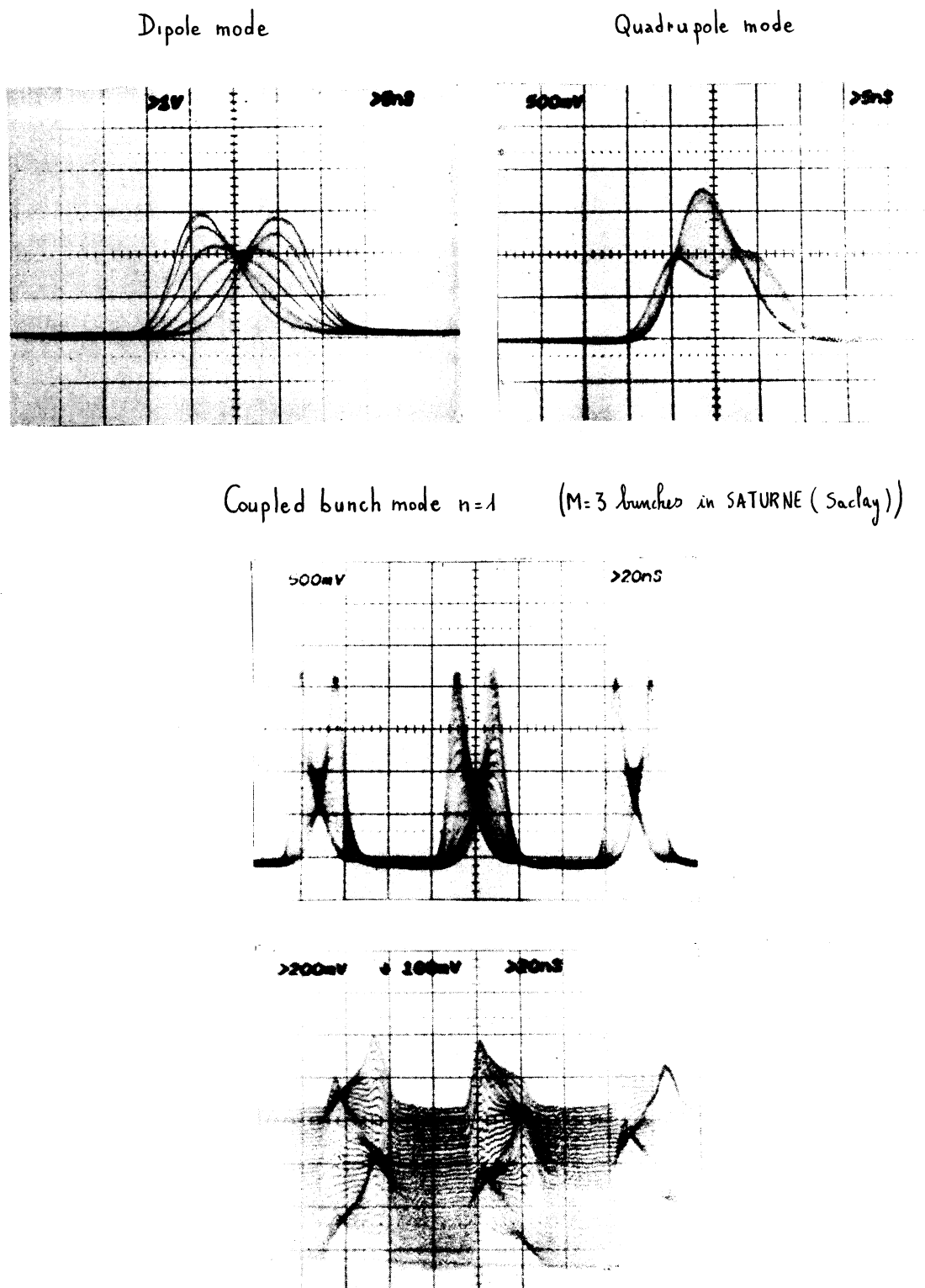


Fig. 16 Experimental observation of bunch oscillations (top) and coupled-bunch mode (bottom) in SATURNE (Saclay)

2.8 Single-bunch instability at high intensity

As stated before, the original theory of F. Sacherer can quite well explain low intensity phenomena that have been observed with bunched beams in a circular machine.

However, in this form, this theory cannot explain other types of single bunch instabilities that have been found.

For instance the "microwave instability", the signature of which is a high frequency signal, shows up in most machines (long proton bunches and short electron bunches), above some threshold current. Boussard's criterion derived from the Keil-Schnell coasting beam stability requirement by using local values of current and momentum spread can predict this threshold quite accurately.

In addition, with increasing current the rate of bunch lengthening due to potential well effect changes suddenly above a threshold current. This "anomalous" bunch lengthening often called "turbulent" bunch lengthening is accompanied by a bunch widening (increase of momentum spread).

An attempt to explain some of the above effects with theory consists of introducing "mode coupling".

2.8.1 Analysis of the instability mechanism

In order to explain the way mode coupling acts, let us go back to the low intensity regime and consider a single perturbation again, the dipole mode for example.

As represented in Fig. 10, once the stationary signal has been subtracted, the single pass signal of the perturbation is an odd function of time. As a consequence, the perturbation spectrum is an odd function of frequency.

When considering a local interaction (2.7.1) the force is exactly the derivative of the signal (signal as seen through a pure inductance). Therefore, the force is an even function of time. It can efficiently drive the perturbation and it leads to a frequency shift proportional to the impedance, according to equation (105).

The same result would apply with a capacitance as well. The force would be the integral of the signal, that is to say an even function of time again and it would drive efficiently the perturbation.

On the other hand, with a pure resistance the force is exactly the signal. This time it has the wrong parity to drive the perturbation (weak differential effect).

Conclusion : an odd perturbation is essentially driven by an even force. Indeed, an even perturbation is essentially driven by an odd force.

Now, let us add two adjacent perturbations, an odd one (dipole $m=1$) and an even one (quadrupole $m=2$) interacting with a general impedance (inductance or capacitance plus resistance).

Each perturbation will interact with the forces that have the right parity to drive them, namely, the reactive part of its self field plus the resistive part of the adjacent perturbation field.

Conclusion : two adjacent perturbations cannot couple via a pure reactance. A resistance is necessary.

Let us notice that resistance contributes an imaginary frequency shift and may cause instability.

2.8.2 Matrix equation of single-bunch modes at high intensity

The starting point is equation (84). Both sides can be multiplied by $J_m(l\omega_0 \hat{\epsilon})$ and integrated over $\hat{\epsilon}$ values.

$$(\omega_c - m\omega_s) \sigma_m(l) = \frac{-2\pi I_m \omega_s}{\omega_0^2 V_T h \cos(\phi_s + \Delta\phi_s)} \sum_p \int \frac{Z_p(p)}{P} \int_0^\infty \frac{d\hat{\epsilon}}{\hat{\epsilon}} J_m(p\omega_0 \hat{\epsilon}) J_m(l\omega_0 \hat{\epsilon}) d\hat{\epsilon} \sigma(p). \quad (122)$$

Then, using the definition (85), one can sum up over m values and express the spectral amplitude at $l\omega_0 + \omega_c$.

$$\sigma(\ell) = \frac{-2\pi I}{\omega_0^2 V_T h \cos(\varphi_s + \Delta\varphi_s)} \sum_p \int \frac{Z_{\parallel}(p)}{p} \left\{ \sum_m \frac{m\omega_s}{\omega_c - m\omega_s} \int_0^\infty \frac{\partial g_0}{\partial \hat{z}} J_m(p\omega_0 \hat{z}) J_m(\ell\omega_0 \hat{z}) d\hat{z} \right\} \sigma(p) . \quad (123)$$

Let us introduce a matrix element $M_{\ell p}$.

$$\sigma(\ell) = \frac{4I}{\pi^2 B^3 V_T h \cos(\varphi_s + \Delta\varphi_s)} \sum_p \int \frac{Z_{\parallel}(p)}{p} M_{\ell p} \sigma(p) . \quad (124)$$

When the bunch has a stationary distribution with parabolic amplitude (25), $M_{\ell p}$ takes the following form

$$M_{\ell p} = 2B \sum_m \frac{m}{\frac{\omega_c}{\omega_s} - m} \int_0^1 J_m(p\pi Bx) J_m(\ell\pi Bx) x dx . \quad (125)$$

Let us examine the method that can be used to solve the above matrix equation (124).

Assume a real coherent frequency ω_c measured in incoherent frequency unit, ω_c/ω_s .

Look for the eigenvalues of the matrix

$$\left[\int \frac{Z_{\parallel}(p)}{p} \right] \left[M_{\ell p} \right] \quad (126)$$

where $\left[\int Z_{\parallel}(p)/p \right]$ is the diagonal matrix associated with the impedance.

Scale the intensity parameter

$$\xi = \frac{4I}{\pi^2 B^3 V_T h \cos(\varphi_s + \Delta\varphi_s)} \quad (127)$$

in order to adjust the eigenvalue to unity.

Assume that the bunch is long enough and use the low frequency imaginary part of the impedance to calculate V_T/V_{RF} and $\Delta = (\omega_s^2 - \omega_{s0}^2)/\omega_{s0}^2$ (equation 62).

Finally, by means of equation (67) or (69) find out the bunch length.

In the following, we apply this method to three special types of impedances, inductive wall or space-charge, narrow-band resistance, broad-band resonator.

2.8.3 Space-charge and inductive-wall modes at high intensity

As it has been already pointed out in section 2.8.1, odd and even perturbations cannot couple since there is no resistive component in the assumed impedance. There is a very weak coupling between perturbations with the same parity. This coupling modifies slightly the C_{mq} 's.

The results are presented in Fig. 17.

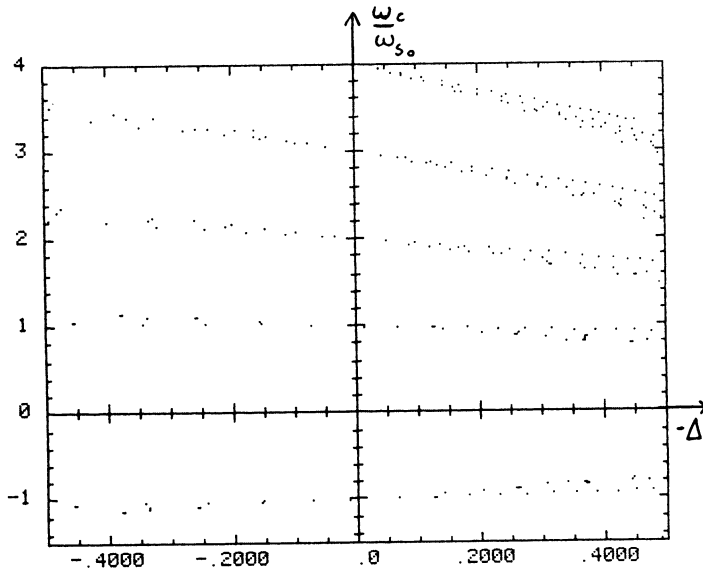


Fig. 17 Coherent frequency shift as a function of the incoherent shift for an inductive impedance

2.8.4 Narrow band resistance

In this section the goal we aim at is to illustrate the resistive coupling. To this end we assume a narrow-band resistance at coherent frequency $\rho\omega_0 + \omega_c$.

$$\oint \frac{Z_{ll}(p)}{p} = 0 \quad \text{except at } p = \pm p_c \quad \text{and} \quad \oint \frac{Z_{ll}(p_c)}{p_c} = - \oint \frac{Z_{ll}(-p_c)}{-p_c} = \oint \frac{R_s}{p_c} . \quad (128)$$

Furthermore, we assume a pair of adjacent perturbations m and $m+1$ for instance.

By using some elementary algebra and the following definitions

$$k_m = \int_0^{+\infty} J_m(p_c \omega_0 \hat{z}) \hat{z} d\hat{z} > 0 , \quad \sigma_m(-p_c) = (-1)^m \sigma_m(p_c)$$

the matrix equation (124) can be reduced to

$$\begin{pmatrix} \sigma_m(p_c) \\ \sigma_{m+1}(p_c) \end{pmatrix} = 4B\varepsilon \int \frac{R_s}{p_c} \begin{pmatrix} 0 & \frac{m k_m}{\frac{\omega_c}{\omega_s} - m} \\ \frac{(m+1) k_{m+1}}{\frac{\omega_c}{\omega_s} - (m+1)} & 0 \end{pmatrix} \begin{pmatrix} \sigma_m(p_c) \\ \sigma_{m+1}(p_c) \end{pmatrix} . \quad (129)$$

The eigenvalues are solutions of a quadratic equation

$$\left(\frac{\omega_c}{\omega_s} - m \right) \left(\frac{\omega_c}{\omega_s} - (m+1) \right) = -C^2 \varepsilon^2 \quad (130)$$

$$C^2 = 16m(m+1)R_s^2 B^2 \frac{k_m k_{m+1}}{p_c^2} .$$

with

The instability threshold is obtained for $\epsilon_{th} = 1/2c$. This threshold depends strongly on the value of ω_c . The instability is efficiently driven when ω_c is such that the product $k_m \cdot k_{m+1}$ is maximum, that is to say $\omega_c \approx \frac{(2m+3)\pi}{\tau_L}$.

Below threshold, the two coherent frequencies are real. The motion is stable. Above threshold, the real part of the coherent frequency ω_c is constant and the imaginary part is positive for one mode (stability) and negative for the other one (instability). Since one mode is unstable, the bunch is unstable.

Results are summarized in Fig. 18a for $m = 1$.

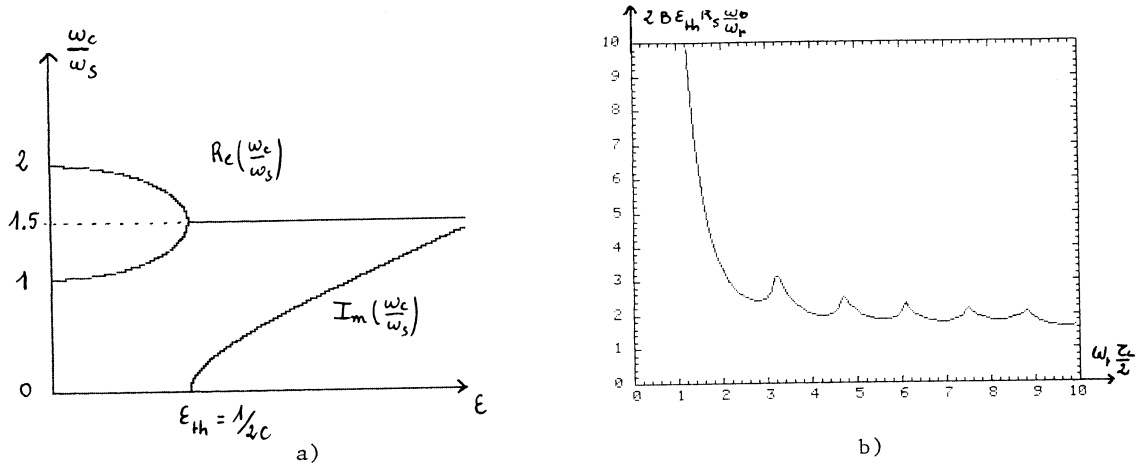


Fig. 18 a) Coherent frequency shift versus intensity for a narrow-band impedance
b) Threshold intensity as a function of the bunch length

At low intensity, we find two modes. The first one at coherent frequency $\omega_c = \omega_s$ is essentially composed of a dipole perturbation. The second one at $\omega_c = 2\omega_s$ consists of a rather pure quadrupole perturbation.

For increasing current, the spacing between the two coherent frequencies gets smaller. Each of the two modes is a mixing of dipole and quadrupole perturbations.

At threshold, the two modes are identical. They are associated with the same coherent frequency $\omega_c = 3\omega_s$. Maximum stable coupling is reached.

For a narrow-band resonator, when including an infinite number of perturbations, the intensity parameter at threshold ϵ_{th} is given by

$$2B\epsilon_{th} R_s \frac{\omega_0}{\omega_r} = \left\{ - \left(\sum_{n=1}^{+\infty} \frac{(2n)^2 k_{2n}}{\left(\frac{\omega_c}{\omega_s}\right)^2 - (2n)^2} \right) \left(\sum_{n=0}^{+\infty} \frac{(2n+1)^2 k_{2n+1}}{\left(\frac{\omega_c}{\omega_s}\right)^2 - (2n+1)^2} \right) \right\}^{-1/2}.$$

In Fig. 18b the above quantity is represented as a function of $\omega_r \tau_L$.

2.8.5 Broad band resonator

Now, we give the results one would obtain with an impedance that consists of a pure resonator of Broad-Band type (Fig. 20). The resonant frequency ω_r (Fig. 19) lies between the maxima of the spectra of modes 22 and 33 ($\omega_{22} \approx 3\pi/\tau_L$ and $\omega_{33} \approx 4\pi/\tau_L$) as obtain with a constant $Z_{ll}(p)/p$ (see Fig. 10).

The solution of the matrix equation of coherent motion (124) is a twofold infinity of modes as shown in Fig. 20. The upper graph gives the coherent frequency ω_c of the modes in ω_{so} unit (vertical axis) as a function of $-\Delta$ (equation (62)) that measures the normalized shift of incoherent frequency squared (horizontal axis) for a long bunch $\omega_r \tau_L \gg 1$. The lower graph gives the same results with $-\epsilon R_s \omega_0 / \omega_r$ along the horizontal axis (equation (127)).

$$\Delta = \frac{\omega_s^2 - \omega_{so}^2}{\omega_{so}^2} = \frac{16 I}{\pi^3 B^3 V_{RF} h \cos \varphi_s} \quad \frac{R_s \omega_0}{Q \omega_r} = \frac{4}{\pi} \frac{V_T}{V_{RF}} \epsilon \frac{R_s \omega_0}{Q \omega_r} . \quad (131)$$

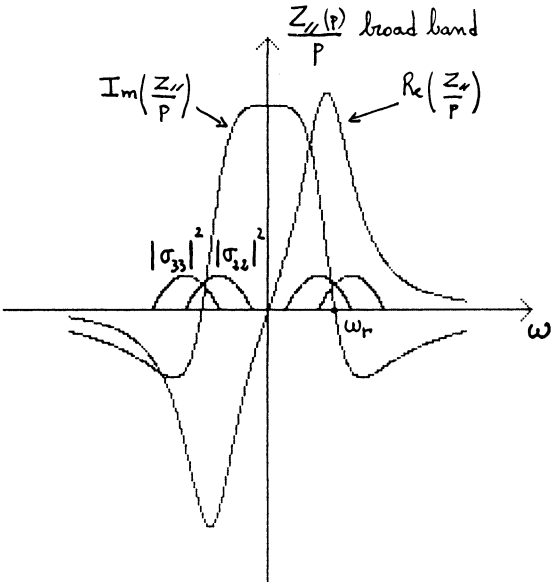


Fig. 19 Broad-band resonator impedance and mode spectra

Below transition "mode coupling" cannot lead to instability. This is the reason why we restrict ourselves to working points with a positive abscissa ($-\Delta > 0$). We are above the transition and because of the low frequency inductance the incoherent frequency decreases for increasing intensity. At very low intensity ($-\Delta \rightarrow 0$), there is no instability, the coherent frequencies are real, they cluster near the integer values of ω_c/ω_{so} . For increasing intensity, some of the coherent frequencies are pulled up, others are pulled down. At sufficiently high intensity for two coherent frequencies to merge, instability appears. In the present example, the lowest threshold occurs at $-\Delta_{th} = .54$. In the interval, $2 < \omega_c/\omega_{so} < 3$ when following the solid curve, we can see that the comments already made in the previous section apply again. At low intensity, we get two modes on the curve. The first one, at coherent frequency $\omega_c \sim 2 \omega_{so}$ is essentially composed of quadrupole perturbation g_{22} . Its spectrum is shown in Fig. 20a. The second one at $\omega_c \sim 3 \omega_{so}$, consists in a rather pure sextupole perturbation g_{33} (Fig. 20c). For increasing current, the spacing between the two coherent frequencies gets smaller and smaller. On one hand, the coherent frequency of the first mode is pulled up because its spectrum overlaps the inductive part of the impedance. On the other hand, the coherent frequency of the second mode is pulled down because its spectrum overlaps the capacitive part of the impedance. Each of the two modes is a mixing of quadrupole and sextupole perturbation. At threshold $-\Delta = -\Delta_{th}$ (Fig. 20b) the two modes are at the same coherent frequency $\omega_c \sim 1.7 \omega_{so}$. Maximum stable coupling is reached.

Obviously, the instability threshold depends on the resonant frequency of the resonator and on its bandwidth.

The example of Fig. 20 is a broad band with a bandwidth $\Delta \approx 1$ about as wide as the mode spectra. In other words the wakefield decay in about a bunch length τ_L . This is the worst situation leading to the lowest thresholds.

For very small bandwidths, only a few lines contribute and the threshold is high.

In Fig. 21, with $-\epsilon R_s \omega_0 / \omega_r$ along the horizontal axis, the result corresponding to a very narrow band resonator at frequency $\omega_r \tau_L = 7.85$ is shown.

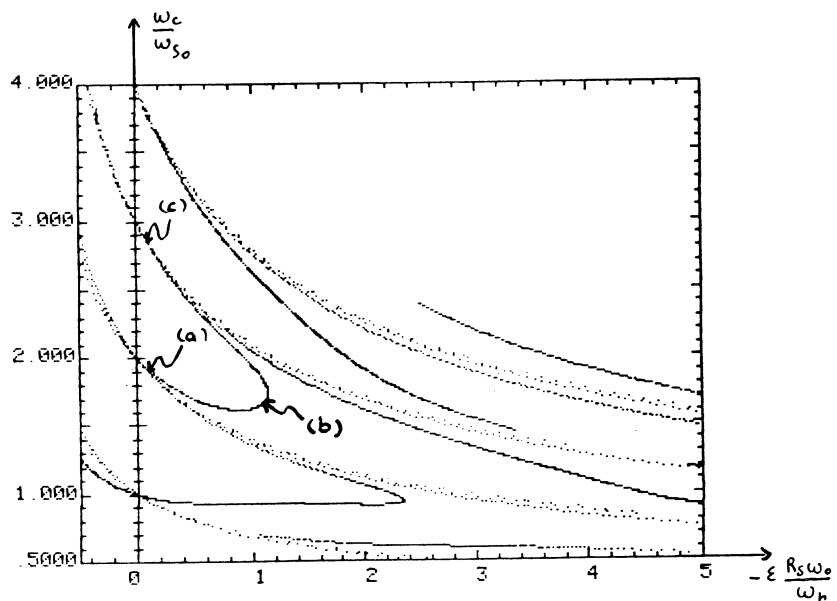
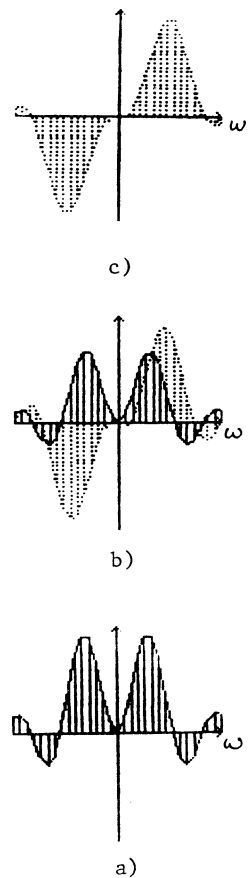
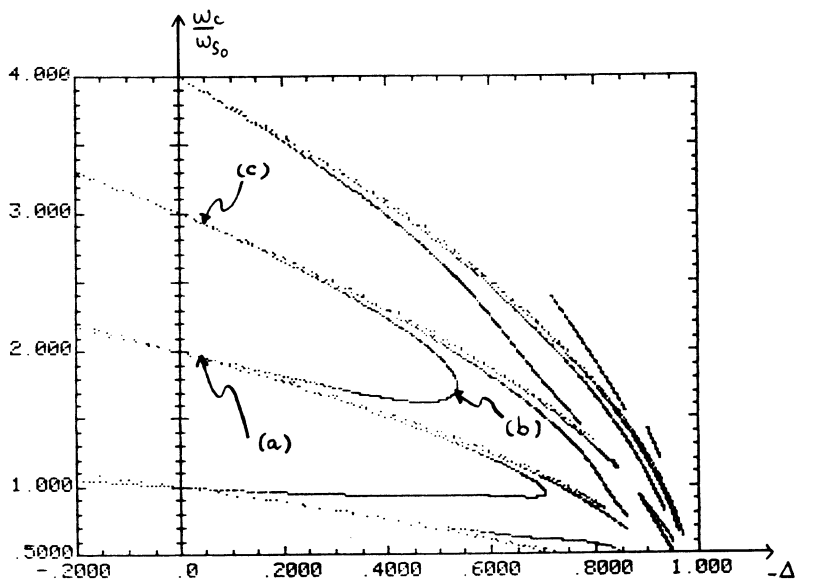


Fig. 20 Coherent-mode frequencies ($m = 1$ to 4) versus incoherent frequency shift (upper) and intensity parameter (lower)
 a) Spectrum of the lowest radial quadrupole mode g_{22}
 b) Coupling between quadrupole and sextupole modes at threshold
 c) Spectrum of the lowest radial sextupole mode g_{33}

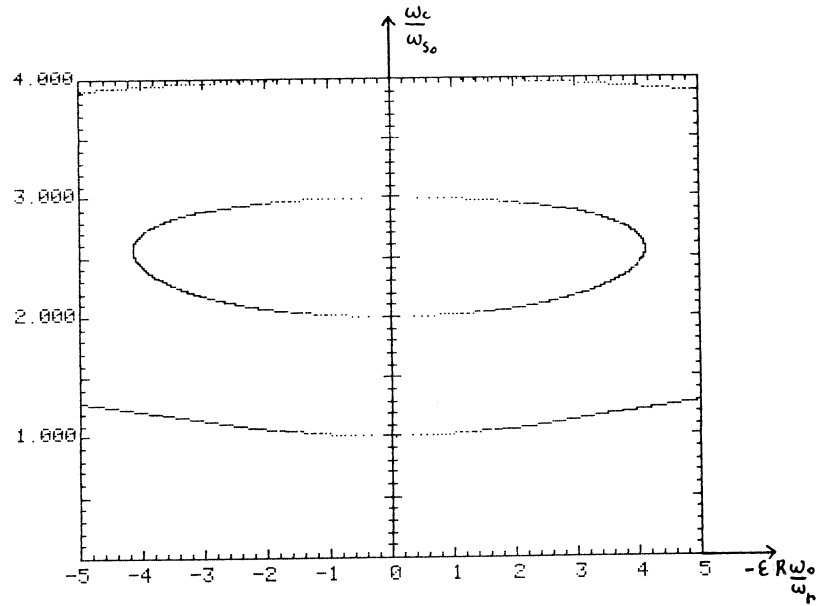


Fig. 21 Coherent-mode frequencies versus intensity for a narrow-band resonator impedance

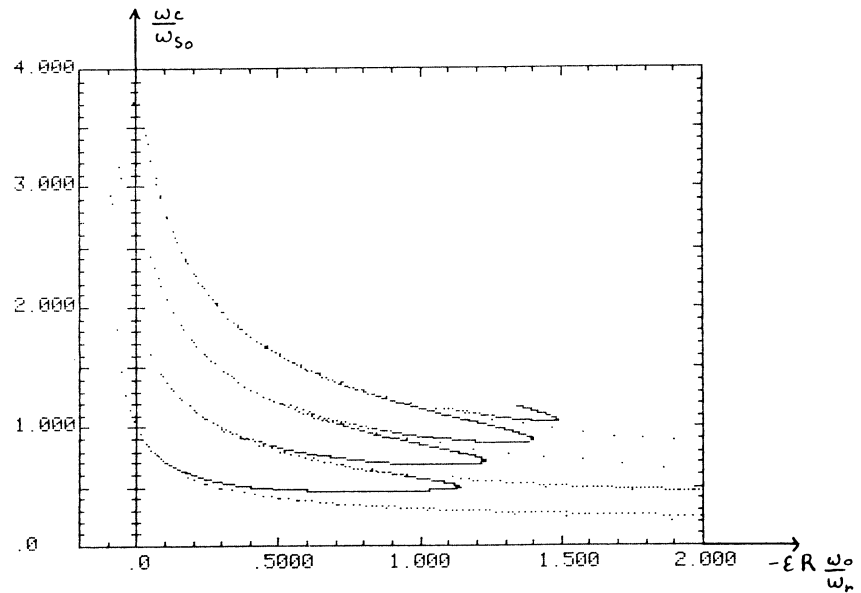


Fig. 22 Coherent-mode frequencies versus intensity for a wide-band resonator impedance

For very large bandwidths, more and more modes lie under the resonance curve and the threshold is higher again (see Fig. 22).

Above transition energy, results corresponding to different resonant frequencies and different bandwidths of the resonator are summarized in Fig. 23.

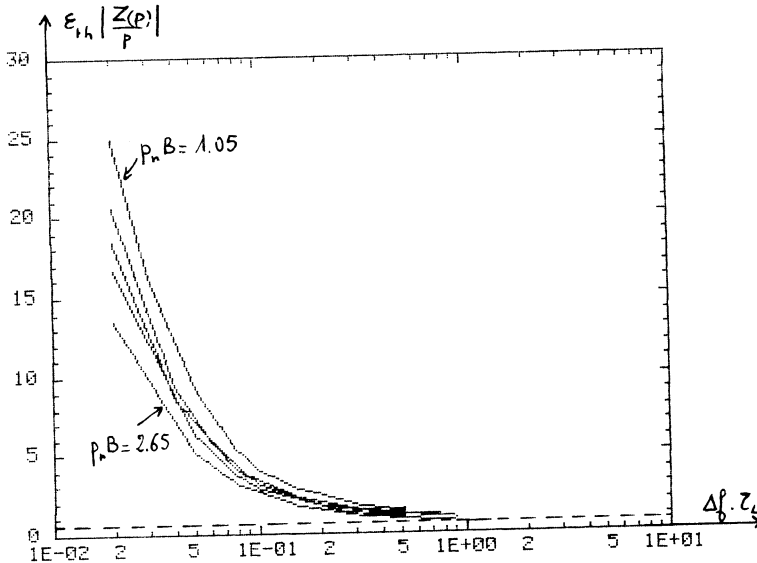


Fig. 23 Normalised threshold intensity parameter versus bandwidth for different resonant harmonic numbers $Pr = \omega_r/\omega_c$

If one defines the peak current \hat{I} and the full-width half-height momentum spread as follows,

$$\hat{I} = \frac{3I}{eB} \quad (132)$$

$$\left(\frac{\Delta p}{p} \right)_{FWHH}^2 = \frac{\omega_s^2 \tau_L^2}{2 \eta^2} \quad (133)$$

then stability requires

$$\epsilon_h \left| \frac{Z(p)}{p} \right| < 0.7 \quad \text{or} \quad \frac{8}{3\pi(0.7)} \frac{\hat{I}}{\omega_0 \eta R \left(\frac{p}{e} \right)} \left| \frac{Z(p)}{p} \right| \leq \left(\frac{\Delta p}{p} \right)_{FWHH}^2 \quad (134)$$

It is interesting to notice that the lowest threshold is equivalent ($8/3\pi \approx 0.7$) to the coasting beam threshold for peak current (D. Boussard criterion). Presumably, the bunch lengthens and widens to remain just below threshold.

2.8.6 Bunch lengthening and widening

For given RF conditions (V_{RF} , k , $\cos \phi_s$) and given impedance, we plan to define the dimensions of the bunch required for stability. Let us recall the following notations

$$\Delta = \frac{\omega_s^2 - \omega_{s0}^2}{\omega_{s0}^2} \quad \text{and} \quad \Delta_0 = \left(\frac{\omega_s^2 - \omega_{s0}^2}{\omega_{s0}^2} \right)_0 = \left(\frac{B}{B_0} \right)^3 \Delta . \quad (135)$$

- Proton case

Let B_0 be the zero intensity bunch β factor. Matching fixes the peak momentum spread and therefore the emittance.

We start increasing current. Because of the potential well effect, the incoherent synchrotron frequency changes (decreases for example). According to equation (69), new matched conditions can be found, same emittance, smaller momentum spread, longer bunch.

$$\left(\frac{B}{B_0}\right)^{-1} = \left(\frac{B}{B_0}\right)^3 + \Delta_0 . \quad (69)$$

This remains valid till we stay below the instability threshold $\Delta < \Delta_{th}$.

Once the threshold is reached, the emittance of the bunch cannot be kept constant. The bunch has to lengthen in order to maintain Δ at threshold. The momentum dimension has to follow to satisfy matched conditions. The bunch widens out. Equations (136), (137) and (138) apply.

$$\left(\frac{B}{B_0}\right)^3 = \frac{\Delta_0}{\Delta_{th}} \quad (136)$$

$$\left(\frac{\epsilon}{\epsilon_0}\right)^6 = (1 + \Delta_{th})^3 \left(\frac{\Delta_0}{\Delta_{th}}\right)^4 \quad (137)$$

$$\left(\frac{\Delta p_p}{(\Delta p_p)_0}\right)^6 = (1 + \Delta_{th})^3 \left(\frac{\Delta_0}{\Delta_{th}}\right)^2 . \quad (138)$$

- Electron case

Radiation damping determines the momentum spread. At zero intensity, matching fixes B_0 and consequently the emittance.

We start increasing current. Potential well decreases the focusing, the momentum spread remains the same, the bunch lengthens according to equation (67), the emittance grows.

$$\frac{B}{B_0} = \left(\frac{B}{B_0}\right)^3 + \Delta_0 \quad (67)$$

$$\frac{\epsilon}{\epsilon_0} = \frac{B}{B_0} . \quad (139)$$

This remains valid till we stay below the instability threshold $\Delta < \Delta_{th}$.

When the threshold is reached, the bunch starts lengthening differently to remain stable. The same equations as for protons (136), (137) and (138) are valid.

Figure 24 gives a qualitative description of the evolution of beam parameters below and at threshold.

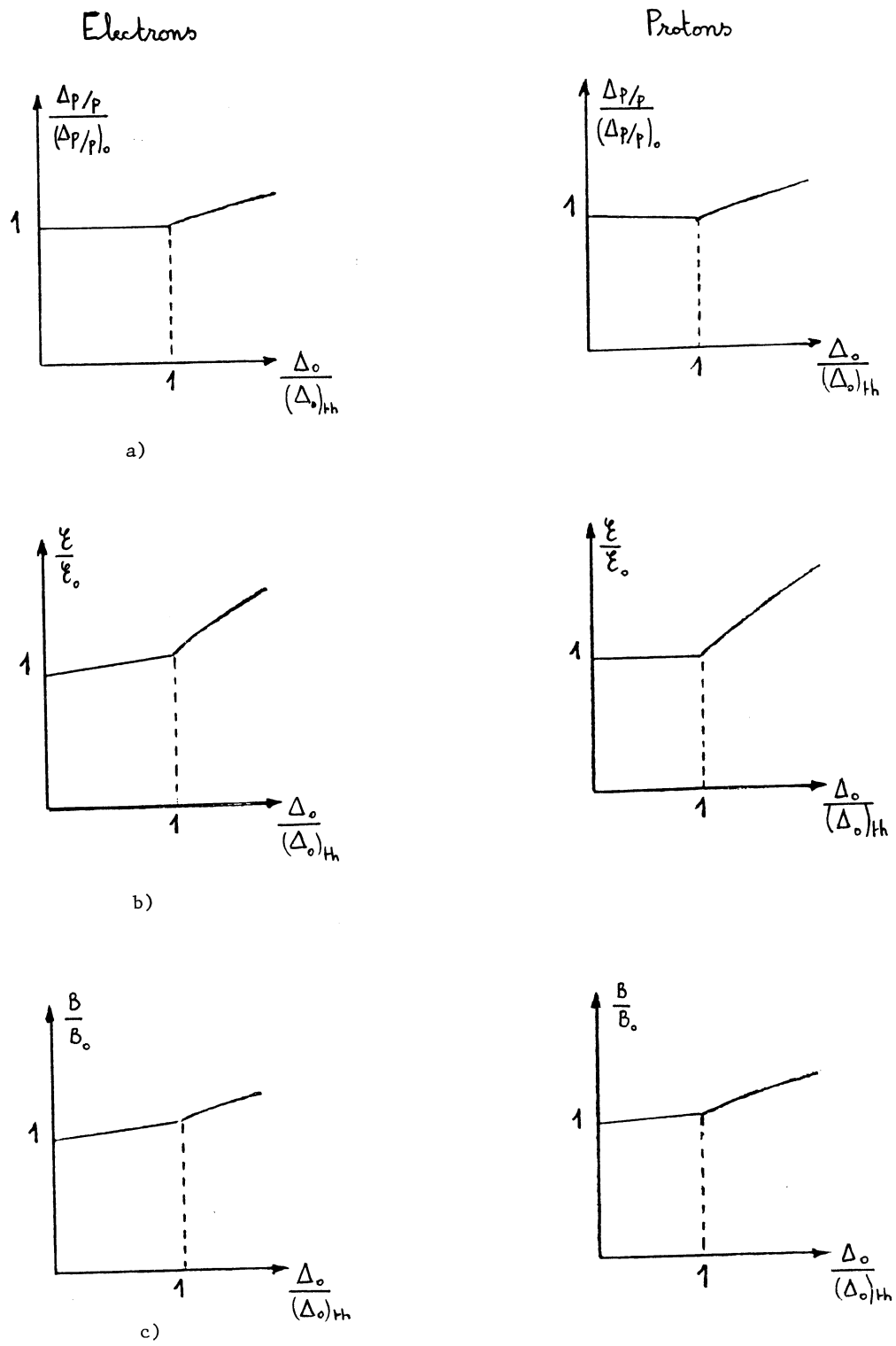


Fig. 24 a) Relative momentum, b) emittance and c) bunch length, versus normalized frequency shift for electrons and protons

3. TRANSVERSE INSTABILITIES

3.1 Preliminary remarks

To deal with transverse instabilities we will follow exactly the same procedure as before. Again we will work in the frequency domain with transverse signal, stationary distribution and perturbation. We will assume a transverse impedance and by means of Vlasov's equation we will describe the coherent motion which consists in eigenmodes of oscillation and coherent frequencies.

Indeed, most of the comments already made in the previous section apply. Therefore, in order to avoid repetitions we will mainly insist on differences between longitudinal and transverse cases.

In the longitudinal case, the instability process is initiated by a perturbation of particle density which creates an electromagnetic field across the beam. Remembering the example of a circular pipe, this electromagnetic field was associated with a return or image current S_w flowing upstream in the wall and uniformly distributed around the beam axis.

In the transverse case, the perturbation consists of a slight transverse displacement of the beam which oscillates from side to side in the external focusing guide field. This time, the wall current S_w is not uniformly distributed around the pipe axis. It is a differential current which flows in opposite directions on either side of the vacuum chamber. This requires a longitudinal electric field E_{\parallel} which varies in strength across the aperture and a transverse dipole magnetic field B_z as shown in Fig. 25. This magnetic field B_z deflects the beam. It can increase the initial displacement (instability) or decrease it (stability).

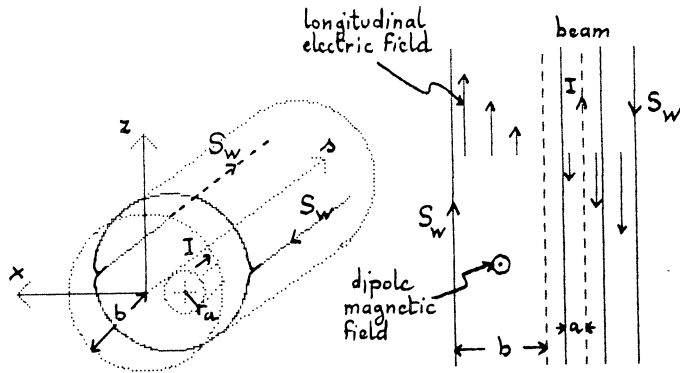


Fig. 25 Beam transversely oscillating in a conducting pipe

Indeed, we could have considered higher-order defects induced by an on-axis beam the transverse dimensions of which change periodically with time (throbbing-beam modes).

In the present lecture, we will restrict ourselves to the study of the effect of the dipolar magnetic field. This is the simplest transverse interaction between the beam and the surroundings.

3.2 Single particle motion

In order to describe the transverse motion of particles in a bunch, one needs four coordinates. Two of them are related to the projection on the longitudinal phase space. We will use again

$(\hat{r}, \hat{\varphi})$ or $(\hat{\psi}_0, \hat{z})$ (see section B.1)

$$z = \hat{z} \cos(\omega_s t + \psi_0) . \quad (140)$$

The second pair of coordinates
 (x, \dot{x}) or $(\varphi, \dot{\varphi})$

corresponds to the projection on one of the two transverse phase spaces (horizontal for instance).

The solution of the equation of unperturbed motion in the transverse plane, will be written

$$x(t) = \hat{x} \cos \varphi(t) . \quad (141)$$

A very important point is that the betatron phase advance per unit of time or betatron frequency

$$\dot{\varphi} = Q \omega \quad (142)$$

depends on the instantaneous momentum deviation of the particle in first order. It can be expanded as follows

$$\dot{\varphi} = Q_0 \left(1 - \xi \frac{dp}{P} \right) \omega_0 \left(1 - \eta \frac{dp}{P} \right) = Q_0 \omega_0 \left(1 - \dot{\tau} \left(1 - \frac{\xi}{\eta} \right) \right) . \quad (143)$$

Q_0 and ω_0 are the transverse wavenumber and the revolution frequency evaluated at synchronous energy.

$$\xi = \frac{dQ}{Q} / \frac{dp}{P} \quad \text{is the machine chromaticity} \quad (144)$$

$$\eta = - \frac{d\omega}{\omega} \quad \text{has been defined in section 2.1 already.}$$

According to the above definitions, the transverse coordinate satisfies

$$\ddot{x} - \frac{\ddot{\varphi}}{\dot{\varphi}} \dot{x} + \dot{\varphi}^2 x = 0 . \quad (145)$$

The second order, Q and ω depend on transverse amplitudes and momentum spread. In the following, we will neglect this dependence. Furthermore, we will assume that the motion in longitudinal plan is stable (no coherent effect).

Here again, we will be mainly interested in the electromagnetic field induced by the beam. Taking this field into account will modify the differential equation of motion (145) of the single particle.

$$\ddot{x} - \frac{\ddot{\varphi}}{\dot{\varphi}} \dot{x} + \dot{\varphi}^2 x = \frac{e}{m_0 \gamma} \left[\vec{E} + \vec{\beta}_c \wedge \vec{B} \right]_{\perp} (t, \theta = \omega_0(t-\tau)) . \quad (146)$$

3.3 Single particle signal

The transverse displacement of a beam can be detected by means of transverse P U electrodes. These are diagnostic equipments allowing us to measure the local beam center of mass position. The signal drawn from an electrode is the product of the longitudinal signal times the transverse position.

Let us assume a perfect P U electrode at angular position Θ in the ring and let us observe the transverse signal $s_{\perp}(t, \theta)$ induced by an off-centered single particle.

By definition we get

$$s_{\perp}(t, \theta) = s_{\parallel}(t, \theta) x(t) = s_{\parallel}(t, \theta) \hat{x} \cos \varphi(t) . \quad (147)$$

In the time domain, $s_{\perp}(t, \theta)$ consists of a series of impulses, the amplitude of which $X(t)$ changes at each passage through the electrode. Integrating equation (143) to get

$$\psi(t) = Q_0 \omega_0 (t - \tau) + \omega_{\xi} \tau + \varphi_0 \quad (148)$$

with $\omega_{\xi} = Q_0 \omega_0 \frac{\xi}{\eta}$ and $\varphi_0 = \varphi(t)$ at time $t = 0$ (149)

and using equation (9) to express $s_{\parallel}(t, \theta)$, one can successively obtain

$$s_{\perp}(t, \theta) = e^{\hat{X}} \cos(\varphi(t)) \sum_k \delta(t - \tau - \frac{\theta}{\omega_0} - \frac{2k\pi}{\omega_0}) \quad (150)$$

$$s_{\perp}(t, \theta) = \frac{e\omega_0}{2\pi} \hat{X} \frac{(e^{j\varphi(t)} + e^{-j\varphi(t)})}{2} \sum_p e^{jp(\omega_0(t-\tau)-\theta)} \quad (151)$$

when using equations (10) and (12)
and finally

$$s_{\perp}(t, \theta) = \frac{e\omega_0}{4\pi} \hat{X} e^{j(Q_0\omega_0 t + \varphi_0)} \sum_{m,p} j^m J_m(((p+Q_0)\omega_0 - \omega_{\xi})\hat{\tau}) e^{j(\omega_{pm} t + m\psi_0 - p\theta)} + C.C. \quad (152)$$

with $\omega_{pm} = p\omega_0 + m\omega_s$. (14)

With the Fourier transform we can pass on to frequency domain.

$$s_{\perp}(\omega, \theta) = \frac{e\omega_0}{4\pi} \hat{X} e^{j\varphi_0} \sum_{m,p} j^m J_m(((p+Q_0)\omega_0 - \omega_{\xi})\hat{\tau}) \delta(\omega - ((p+Q_0)\omega_0 + m\omega_s)) e^{j(m\psi_0 - p\theta)} + C.C. \quad (153)$$

The single particle spectrum is a line spectrum at frequencies $(p+Q_0)\omega_0 + m\omega_s$. Around every betatron line $(p+Q_0)\omega_0$ there is an infinite number of synchrotron satellites the amplitude of which is given by the Bessel function $J_m(((p+Q_0)\omega_0 - \omega_{\xi})\hat{\tau})$. It is important to notice that the spectrum is centered around ω_{ξ} . This is one of the fundamental differences between transverse and longitudinal cases. For standard machines, the uncorrected chromaticity ξ is negative. Therefore, according to definition (149), ω_{ξ} is a negative frequency above transition energy and a positive frequency below.

3.4 Distribution of particles

The next step consists of gathering particles to form a bunch. To this end, we introduce a distribution function $\Psi(\psi, \hat{\tau}, \varphi, \hat{X}, t)$ that is split into two different parts, a stationary distribution and a perturbation.

3.4.1 Stationary distribution

In the absence of perturbation \hat{X} and $\hat{\tau}$ are constant during the motion. Therefore the stationary part is a realistic function of the two peak amplitudes $\Psi_0(\hat{x}, \hat{\tau})$. We will assume no correlation between transverse and longitudinal planes and we will write the stationary part as the product

$$\Psi_0 = g_0(\hat{\tau}) f_0(\hat{x}) \quad (154)$$

of two stationary distributions, one for each phase space.

$g_o(\hat{z})$ and $f_o(\hat{x})$ can be one of the functions already suggested in the previous section ((25) through (28)) for instance

$$\int g_o(\hat{z}) \hat{z} d\hat{z} = \frac{1}{2\pi} \quad \int f_o(\hat{x}) \hat{x} d\hat{x} = \frac{1}{2\pi} . \quad (155)$$

In the following, our numerical examples will assume a water bag distribution (28) in the longitudinal plane.

Since on an average, the beam center of mass is on axis, the transverse signal as well as the transverse dipole magnetic field induced by the stationary distribution are null.

$$S_{\perp}(t, \theta) = N \int s_{\perp}(t, \theta) \Psi_o(\hat{z}, \hat{x}) \hat{z} \hat{x} d\hat{z} d\hat{x} d\phi_o d\psi_o = 0 \quad (156)$$

N is the number of particles per bunch.

Indeed, because of the current, there is some space charge quadrupolar magnetic field that adds to the external guide field and that changes transverse focusing. The incoherent Q value is different from Q_o (from now on, we will assume that the effective transverse tune is Q , and we will change Q_o into Q in the equations). Nevertheless this is not the type of field we are concerned with in this section.

3.4.2 Perturbation

In order to get some dipole field, we introduce a density perturbation $\Delta\Psi$ that simulates a beam center-of-mass displacement along the bunch. The mathematical form of the perturbation is suggested by the single particle signal. As a matter of fact, because of the integral over Ψ_o and ψ_o , the signal induced would be null unless one introduces the complex conjugate of $\exp j(\Psi_o + m\psi_o)$ in the expression of $\Delta\Psi$.

So, in considering a single value of m , let us write the perturbation as follows :

$$\Delta\Psi = h_m(\hat{z}, \hat{x}) e^{-j(\Psi_o + m\psi_o)} e^{j\Delta\omega_{cm}t} \quad (157)$$

with $\Delta\omega_{cm} = \omega_c - m\omega_s$.

Then, in the time domain, the signal takes the following form:

$$S_{\perp}(t, \theta) = \frac{e\omega_o}{4\pi} N \int \hat{x} \sum_p j^m J_m[((p+Q)\omega_o - \omega_s)\hat{z}] h_m(\hat{z}, \hat{x}) e^{-j(p\theta)} e^{j((p+Q)\omega_o + \omega_s)t} \hat{z} \hat{x} d\hat{z} d\hat{x} d\phi_o d\psi_o . \quad (158)$$

In the frequency domain,

$$S_{\perp}(\omega, \theta) = \frac{4\pi^2 I}{2} \sum_p e^{-jp\theta} \sigma_m(p) \delta(\omega - (\omega_c + (p+Q)\omega_o)) \quad (159)$$

$$\text{with } \sigma_m(p) = j^m \int h_m(\hat{z}, \hat{x}) J_m[((p+Q)\omega_o - \omega_s)\hat{z}] \hat{x}^2 \hat{z} d\hat{z} d\hat{x} \quad (160)$$

we obtain a line spectrum at frequencies $\omega = (p+Q)\omega_o + m\omega_s$. In comparison with the rich spectrum of the single particle, a single synchrotron satellite remains. The perturbation is coherent with respect to satellite number m .

By means of the perturbation, we have arranged the transverse initial conditions of the particles in the bunch. Particles on a given synchrotron orbit \hat{x} have the same peak betatron amplitude \hat{x} . This is included in $h_m(\hat{z}, \hat{x})$. Furthermore, their betatron phase and their synchrotron phase are chosen in order to satisfy

$$\Psi_o + m\psi_o = \text{constant} .$$

The result of this perturbation is that the position of the center of mass changes along the bunch.

We have also assumed that, in phase space, the distribution does not rotate at incoherent frequency $Q\omega_0 + m\omega_s$ exactly but at frequency $Q\omega_0 + \omega_c$. The goal we aim at consists in finding out the values of the coherent betatron frequency shift $\Delta\omega_{cm}$. Its imaginary part will tell us whether the perturbation will increase or will be damped.

We will come back to the physical meaning of $h_m(\hat{z}, \hat{x})$ when we describe the coherent modes of oscillation later on.

As was the case for longitudinal instabilities, we will distinguish two regimes.

At low intensity, the coherent betatron frequency shift will remain small when compared to the incoherent synchrotron frequency ω_s .

$$\Delta\omega_{cm} \ll \omega_s . \quad (161)$$

Therefore, two adjacent perturbations associated with two successive values of m oscillate independently. One can study them separately (equation (157)).

On the other hand, for increasing current, the frequency shifts get larger and it is necessary to sum up several elementary perturbations

$$\Delta\Psi = \sum_m h_m(\hat{z}, \hat{x}) e^{-j(\Psi_0 + m\psi_0)} e^{j(\omega_c - m\omega_s)t} . \quad (162)$$

3.5 Transverse coupling impedance

Because of the initial slight displacement of the beam which oscillates from side to side in the external focusing field, we get a differential current which creates a transverse dipole field. This field perturbs the particle motion.

3.5.1 Definition of the transverse coupling impedance

As previously in the case of the longitudinal plane, we introduce a key parameter of the machine, the transverse coupling impedance $Z_\perp(\omega)$ which gathers all the characteristics of the electromagnetic response of the machine to a passing particle. The coupling impedance allows us to express the transverse field in terms of transverse signal:

$$\left[\vec{E} + \vec{\beta} c \wedge \vec{B} \right]_\perp (\vec{r}, \theta) = \frac{-i\beta}{2\pi R} \int Z_\perp(\omega) S_\perp(\omega, \theta) e^{j\omega t} d\omega \quad (163)$$

$Z_\perp(\omega)$ is expressed in ohm/m.

3.5.2 Transverse coupling impedance of a circular machine

The main components of the transverse impedance of a standard circular machine are listed hereunder and sketched in Fig. 26.

a) resistive wall component

Peaked at low frequencies, it is the principal source of transverse instabilities. When assuming a thick wall vacuum chamber, the impedance can be written

$$Z_{R.W.}(\omega) = (1 + j) \frac{R}{b^3} Z_0 S_0^* \left(\frac{\omega_0}{\omega} \right)^{1/2} \quad (164)$$

with the same notations as in equation (49).

b) parasitic resonators

High Q resonances can be found in RF cavities, septum tanks and kicker tanks.

c) broad band impedance

The broad band component of the impedance takes into account the numerous cross section changes of the vacuum chamber. It can be roughly derived from the longitudinal broad-band impedance (equations (51) through (54)) as follows.

$$Z_{\perp \text{B.B.}}(\omega) = \frac{2c}{b^2} \frac{Z_{\parallel}(\omega)}{\omega} . \quad (165)$$

In fact, the above convenient relationship between $Z_{\perp}(\omega)$ and $Z_{\parallel}(\omega)/\omega$ is strictly valid for the resistive wake in a round pipe, at frequencies well below the pipe cut-off frequency. It is a quite good approximation as far as the broad-band impedance is concerned. It does not apply for other components of a machine impedance.

Because of equation (165), $Z_{\perp}(\omega)$ has the same form as $Z_{\parallel}(\omega)/\omega$ (see Fig. 26). It is interesting to notice that the transverse BB impedance varies like b^{-2} . In other words, it gets larger when the pipe radius is reduced.

d) space charge component

When a round beam of radius a circulates in a round pipe of radius b , the space charge component is given by

$$Z_{\perp \text{S.C.}}(\omega) = - \frac{1}{\beta_0^2 \gamma_0^2} \left(\frac{1}{a^2} - \frac{1}{b^2} \right) . \quad (166)$$

It is a negative inductance that can be large for low β particles.

The actual impedance seen by the beam is the sum of the components listed above.

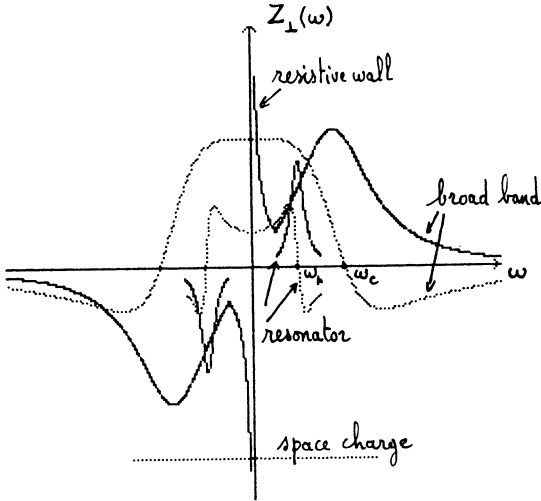


Fig. 26 Qualitative description of transverse impedances for various components (full line = real part, dotted line = imaginary part)

3.6 Equation of coherent motion

We consider a distribution function that sums up a stationary part Ψ_0 (equation (154)) and a perturbation $\Delta\Psi$ (equation (162)).

$$\Psi = q_0(\hat{z}) f_0(\hat{x}) + \sum_m h_m(\hat{z}, \hat{x}) e^{-j(\varphi_0 + m\psi_0)} e^{j(w_c - mw_s)t} . \quad (167)$$

Then, we use Vlasov's equation

$$\frac{\partial \Psi}{\partial t} + \frac{\partial \Psi}{\partial \hat{z}} \dot{\hat{z}} + \frac{\partial \Psi}{\partial \psi_0} \dot{\psi}_0 + \frac{\partial \Psi}{\partial \hat{x}} \dot{\hat{x}} + \frac{\partial \Psi}{\partial \hat{\chi}} \dot{\hat{\chi}} = 0 \quad (168)$$

and we drop second order terms with respect to the perturbation in order to end up with

$$\int \sum_m (\omega_c - m\omega_s) h_m(\hat{z}, \hat{x}) e^{-j(\phi_0 + m\psi_0)t} e^{j(\omega_c - m\omega_s)t} = -g_0(\hat{z}) \frac{\partial f_0}{\partial \hat{x}} \dot{\hat{x}} . \quad (169)$$

In the right hand side of the linearized Vlasov's equation, it is $g_0(\hat{z})$ but not $\frac{\partial g_0}{\partial \hat{x}}$ that appears. This is the reason why a water-bag bunch can be assumed in the present case.

The expression of $\dot{\hat{x}}$ can be drawn from single particle equation of motion (146).

$$\dot{\hat{x}} = -\frac{\sin \psi}{\dot{\psi}} F_c = -\frac{\sin \psi}{\dot{\psi}} \frac{e}{m_0 c} [\vec{E} + \vec{B}_c \wedge \vec{B}]_{\perp} (t, \theta = \omega_0(t-\tau)) . \quad (170)$$

In the right hand side, the coherent transverse electromagnetic "force" F_c can be written

$$F_c = -\frac{1 \beta e}{2\pi R m_0 c} \sum_{m, p} Z_{\perp}(p) \sigma_m(p) e^{-j p \omega_0(t-\tau)} e^{j((p+Q)\omega_0 + \omega_c)t} \quad (171)$$

when equations (163), (159) and (160) are used.

After F_c has been combined with $\sin \psi$ and $\exp j((p+Q)\omega_0 - \omega_{\xi})\tau$ has been developed according to equation (12), one gets

$$\dot{\hat{x}} = -\frac{e\pi I}{2m_0 c \gamma Q} \sum_{m, p} Z_{\perp}(p) \sigma_m(p) J_m[j((p+Q)\omega_0 - \omega_{\xi})\hat{z}] e^{-j(\phi_0 + m\psi_0)\hat{z}} e^{j(\omega_c - m\omega_s)t} . \quad (172)$$

This allows us to rewrite equation (169)

$$\int h_m(\hat{z}, \hat{x}) (\omega_c - m\omega_s) = \frac{e\pi I}{2m_0 c \gamma Q} \sum_p Z_{\perp}(p) \sigma(p) \int^m J_m[j((p+Q)\omega_0 - \omega_{\xi})\hat{z}] g_0(\hat{z}) \frac{\partial f_0}{\partial \hat{x}} \quad (173)$$

where $\sigma(p) = \sum_m \sigma_m(p)$ (174)

is the amplitude of the spectrum of the signal induced by the perturbation at frequency $(p+Q)\omega_0 + \omega_c$.

Both sides of equation (173) can be multiplied by \hat{x} and integrated over \hat{x} values. In the right hand side the integral is easy to perform

$$\int_0^\infty \frac{\partial f_0}{\partial \hat{x}} \hat{x}^2 d\hat{x} = -2 \int_0^\infty f_0(\hat{x}) \hat{x} d\hat{x} = \frac{-1}{\pi} . \quad (175)$$

It leads to

$$\int (\omega_c - m\omega_s) \int_0^\infty h_m(\hat{z}, \hat{x}) \hat{x}^2 d\hat{x} = \frac{-eI}{2m_e c \gamma Q} \sum_p Z_{\perp}(p) \sigma(p) \int J_m[((p+Q)\omega_o - \omega_\xi) \hat{z}] g_o(\hat{z}) . \quad (176)$$

It is important to notice that the transverse stationary function $f_o(x)$ has disappeared. Only the longitudinal function $g_o(z)$ remains in the equation. The problem we are dealing with concerns the beam center of mass essentially. On an average, the detailed betatron motion of individual particles around the center of mass can be disregarded.

The same comments must apply to the perturbation $h_m(z, x)$. As a matter of fact, the quantity of interest is the averaged peak betatron amplitude $\hat{X}_m(z)$ associated with a given synchrotron orbit \hat{z} .

$\hat{X}_m(z)$ can be defined as follows.

$$g_o(z) \hat{X}_m(z) = \int_0^\infty h_m(z, x) \hat{x}^2 dx . \quad (177)$$

The final form of the equation of coherent motion of a single bunch is

$$\int (\omega_c - m\omega_s) \hat{X}_m(z) = \frac{-eI}{2m_e c \gamma Q} \sum_p Z_{\perp}(p) \sigma(p) \int J_m[((p+Q)\omega_o - \omega_\xi) \hat{z}] . \quad (178)$$

From equation (160), the new form of $\sigma_m(p)$ (see equation (174)) is

$$\sigma_m(p) = \int_0^\infty J_m[((p+Q)\omega_o - \omega_\xi) \hat{z}] g_o(\hat{z}) \hat{X}_m(\hat{z}) \hat{z} d\hat{z} . \quad (179)$$

For transverse motion, equation (178) replaces equation (84).

3.7 Coherent modes of oscillation

The general properties of the solutions as well as the different ways to solve equation (178) have been already described in section 2.6. We will develop the eigenvalue method for instance.

Then, both sides of equation (178) are multiplied by $\int J_m[((l+Q)\omega_o - \omega_\xi) \hat{z}] g_o(\hat{z}) \hat{z} d\hat{z}$ and integrated over \hat{z} values.

$$\int (\omega_c - m\omega_s) \sigma_m(l) = \frac{-eI}{2m_e c \gamma Q} \sum_p Z_{\perp}(p) \sigma(p) \int_0^\infty J_m[((p+Q)\omega_o - \omega_\xi) \hat{z}] J_m[((l+Q)\omega_o - \omega_\xi) \hat{z}] g_o(\hat{z}) \hat{z} d\hat{z} . \quad (180)$$

3.8 Low intensity coherent modes of oscillation

We are assuming a low intensity bunch interacting with the different components of the impedance of a ring. A single value of m is retained in the perturbation (157).

We define the matrix element

$$K_{lp}^m = \frac{eI}{2m_e c \gamma Q} (Z_{\perp}(p)) \int_0^\infty J_m[((l+Q)\omega_o - \omega_\xi) \hat{z}] J_m[((p+Q)\omega_o - \omega_\xi) \hat{z}] g_o(\hat{z}) \hat{z} d\hat{z} \quad (181)$$

and rewrite equation (180):

$$(\omega_{c_m} - m\omega_s) \sigma_m(l) = \sum_p K_{l_p}^m \sigma_m(p) . \quad (182)$$

When comparing the $K_{l_p}^m$'s associated with transverse (181) and longitudinal (103) coherent motions, one can draw two conclusions.

First, the value $m=0$ is allowed now.

Second, in the integral $\partial g_0 / \partial \hat{\epsilon}$ is replaced by $g_0(\hat{\epsilon})$, which means that in the transverse case the water-bag bunch (28) leads to results very similar to the ones obtained for the bunch with parabolic amplitude (25) in the longitudinal case. This is the main reason for choosing these two particular distributions.

3.8.1 Local interaction space charge or inductive walls

In this example $\int Z_1(p)$ is real and constant.

Most of the comments already made in section 2.7.1 apply again. Results for the water bag bunch are shown in Fig. 27. At the top, the spectra of the low order coherent modes mq are centered around ω_ξ ; below are the corresponding PU signals (several passings superimposed) for a finite chromaticity ($\omega_E \tau_L = 3\pi/4$) and for zero chromaticity. At the bottom the coherent peak betatron amplitude (equation (178)) as a function of $\hat{\epsilon}$.

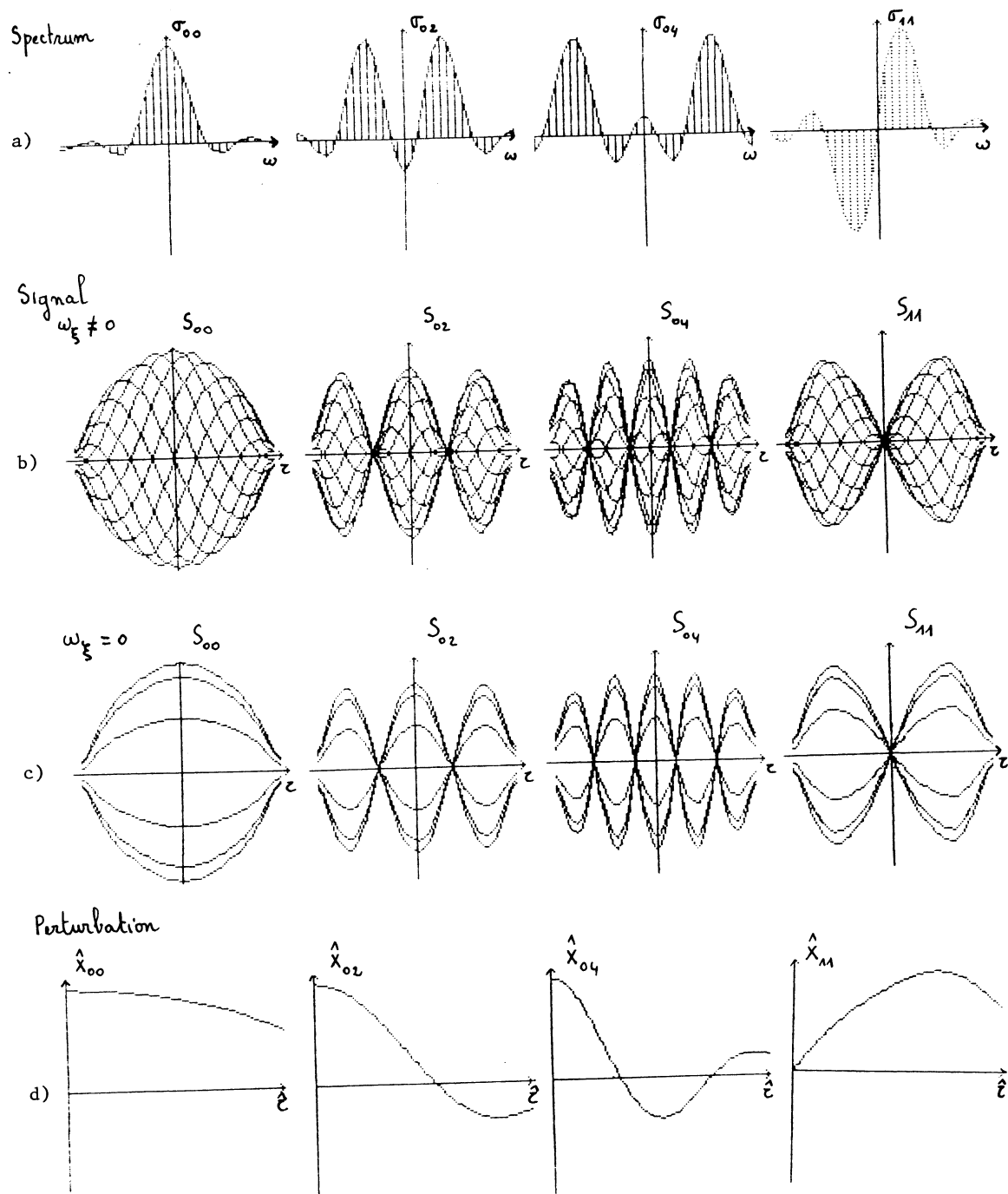
The coherent frequency shifts can be written

$$(\omega_{c_{mq}} - m\omega_s) = \frac{eI}{4\pi m_e c \gamma Q_B} C_{mq} \left(\int Z_1(\omega_\xi) \right) . \quad (183)$$

The values of the C_{mq} are listed in Fig. 27. The largest one corresponds to mode 00 ($C_{00} = 1.09$, dipole mode) that consists of a quite rigid oscillation with the same amplitude \hat{x} for all the ω_ξ in the bunch. The quadrupole mode $m=q=1$ ($C_{11} = 0.46$) is about two times less sensitive. This is due to the fact that particles at bunch center have no coherent response $\hat{x}_{11}(0) = 0$ and do not contribute to the motion.

Because of the special form of the impedance, the shifts are real and motion is stable. A resistance is needed to drive an instability.

Equation (183) is not strictly limited to space charge or inductive walls. It applies to any type of interaction (reactance plus resistance) provided the impedance is sufficiently smooth over the mode spectrum.



$$C_{oo} = 1.1$$

$$C_{o2} = .29$$

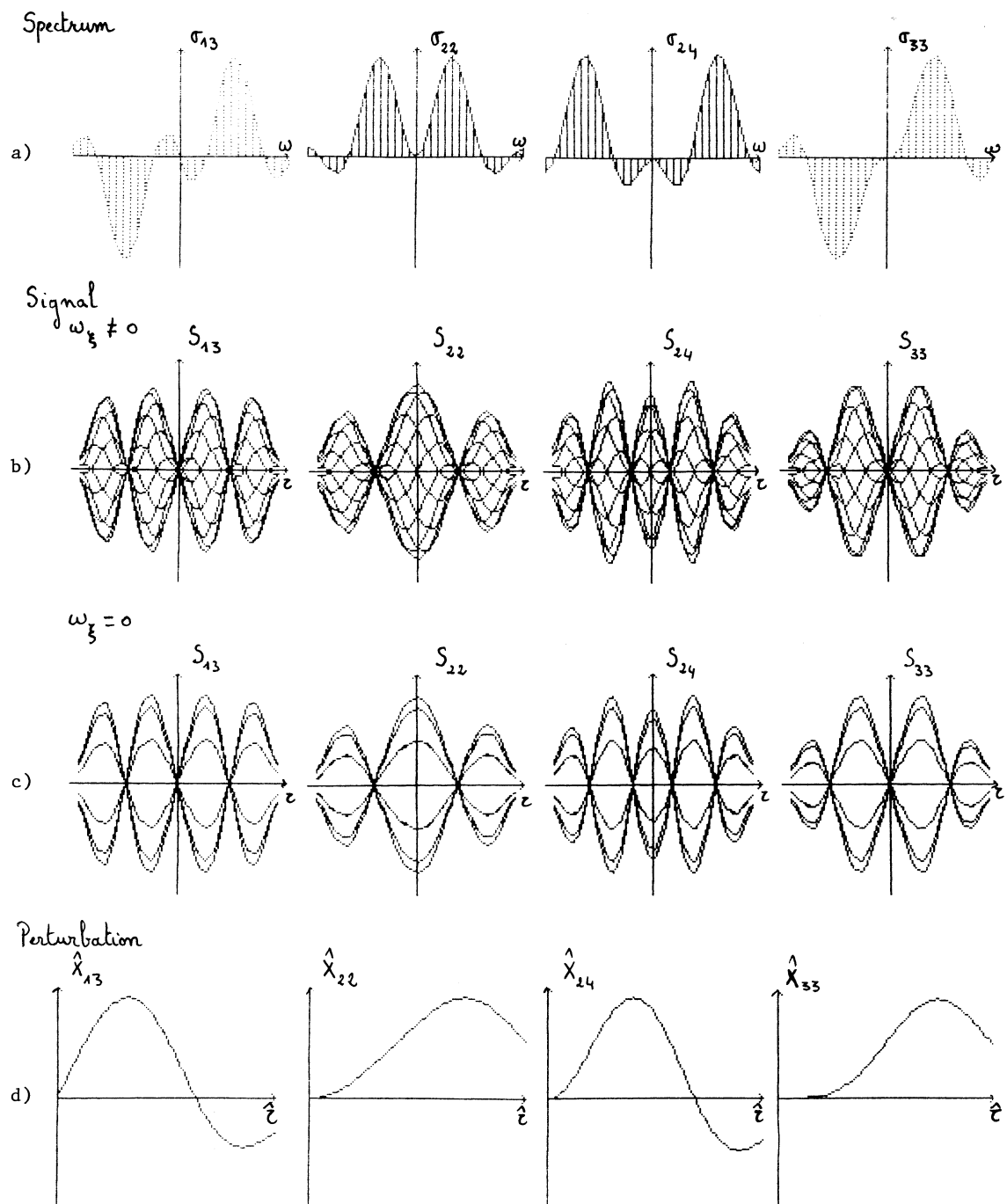
$$C_{o4} = .17$$

$$C_{11} = .46$$

Dipole mode

Quadrupole mode

Fig. 27 Transverse oscillations with mode numbers m, n for a parabolic bunch in an inductive impedance; a) spectrum, b) and c) signals with and without chromaticity respectively, and d) perturbation amplitude



$$C_{13} = .21$$

$$C_{22} = .31$$

$$C_{24} = .17$$

$$C_{33} = .23$$

Fig. 27 (continued)

In Fig. 28, we have sketched an example of stable interaction for which equation (183) is valid. The spectrum of mode σ_{∞} is drawn with a rather large and positive value of ω_{ξ} ($\omega_{\xi} \gg 2\pi/c_s$) so that it does not overlap the low frequency region where the resistive wall impedance is peaked. We are above transition with $\xi > 0$ or below transition with $\xi < 0$.

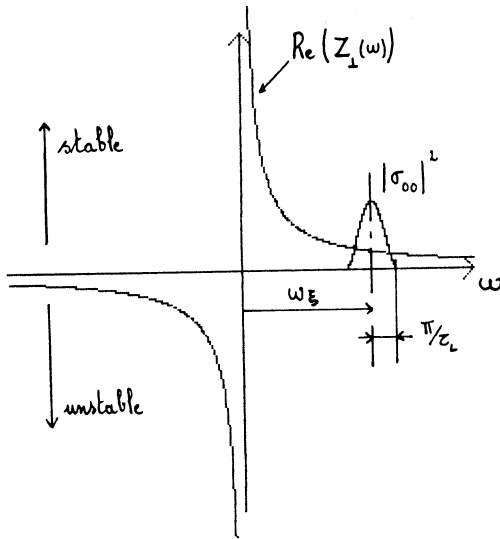


Fig. 28 Stabilisation of resistive-wall instability by chromaticity (for $m = 0$ mode)

A negative ω_{ξ} would lead to instability.

3.8.2 Parasitic high Q resonators - coupled bunch modes

Let us imagine a very narrow band object, so that the motion is driven by a single line at $(p+Q)\omega_0 + \omega_c$. Then, the matrix equation reduces to

$$(\omega_c - m\omega_s) \sigma_m(l) = K_{lp}^m \sigma_m(p) . \quad (184)$$

The sum over p values has disappeared. For every m , a single mode is a solution of equation (184):

coherent frequency

$$\omega_{cm} = m\omega_s + \frac{eI}{2m_0c\gamma Q} \left(\int J_m \left[((p+Q)\omega_0 - \omega_{\xi}) \hat{z} \right] g_o(\hat{z}) \hat{z} d\hat{z} \right) , \quad (185)$$

spectrum

$$\sigma_m(p) = 1 \quad (186)$$

$$\sigma_m(l) = \frac{\int_0^\infty J_m \left[((l+Q)\omega_0 - \omega_{\xi}) \hat{z} \right] J_m \left[((p+Q)\omega_0 - \omega_{\xi}) \hat{z} \right] g_o(\hat{z}) \hat{z} d\hat{z}}{\int_0^\infty J_m \left[((p+Q)\omega_0 - \omega_{\xi}) \hat{z} \right] g_o(\hat{z}) \hat{z} d\hat{z}} , \quad (187)$$

perturbation (see equation (178))

$$\hat{x}_m(\hat{z}) \propto J_m \left[((p+Q)\omega_0 - \omega_\xi) \hat{z} \right]. \quad (188)$$

A resistance is needed in order to get an imaginary frequency shift

$$I_m(\omega_c) \propto I \operatorname{Re}(Z_{\perp}(p)) \int_0^\infty J_m^2 \left[((p+Q)\omega_0 - \omega_\xi) \hat{z} \right] g_0(\hat{z}) \hat{z} d\hat{z}. \quad (189)$$

The integral is always positive. As a consequence a negative resistance (negative frequency region) leads to unstable motion.

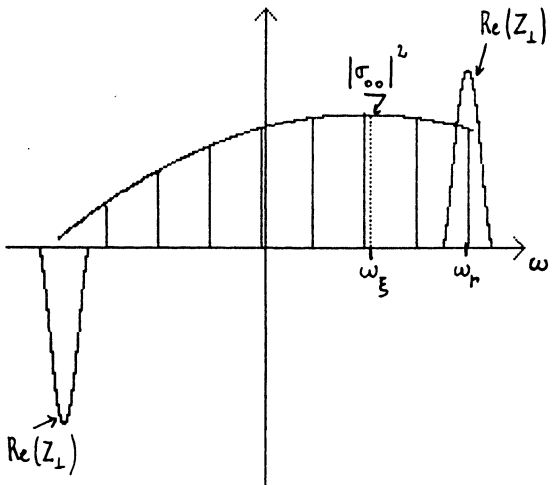


Fig. 29 Stabilisation of transverse instability, due to narrow-band impedance, by chromaticity (for $m = 0$ mode)

In Fig. 29, the picture of a stable scenario is shown.

Let ω_r be the resonant frequency, then, for the water-bag bunch, an equivalent form of equation (185) is

$$(\omega_{c_m} - m\omega_s) = \frac{1}{(|m|+1)} \frac{eI}{4\pi m_0 c Q} \left(\int Z_{\perp}(p) F_m \left((\omega_\xi - (p+Q)\omega_0 - m\omega_s) \frac{z_c}{z} \right) dz \right). \quad (190)$$

The form factor F_m is plotted in Fig. 30

$$F_m(x) = \frac{2(|m|+1)}{x^2} \int_0^x J_m(u) u du \quad (191)$$

Up to now, a single bunch has been assumed. As shown previously in the longitudinal case, if M equidistant bunches are present in the ring, one can consider M possibilities of coupled bunch coherent motion. With the index n running from 0 to $M-1$, coupled bunch mode n corresponds to a phase shift of $n2\pi/M$ between the coherent perturbations of two successive bunches.

Every M^{th} line occurs at

$$\omega = (n + pM + Q)\omega_0 + \omega_c \quad (192)$$

but with an amplitude M times larger. As a consequence, the frequency shift (190) must be multiplied by M .

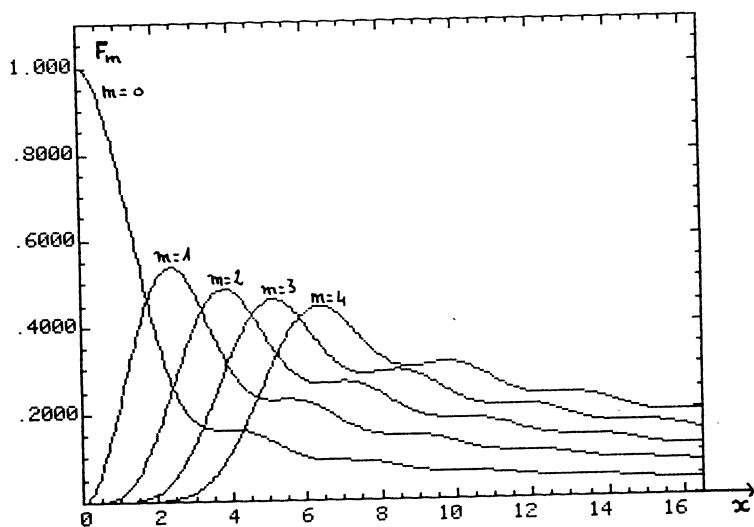


Fig. 30 Form factors F_m for different modes m of transverse-bunch oscillation

3.8.3 Resistive wall component

As we have seen previously, the resistive part of $Z_1(p)$ causes instability for negative resistance (negative frequency region) and damping for positive resistance (positive frequency region).

The resistive wall interaction can be split into two parts.

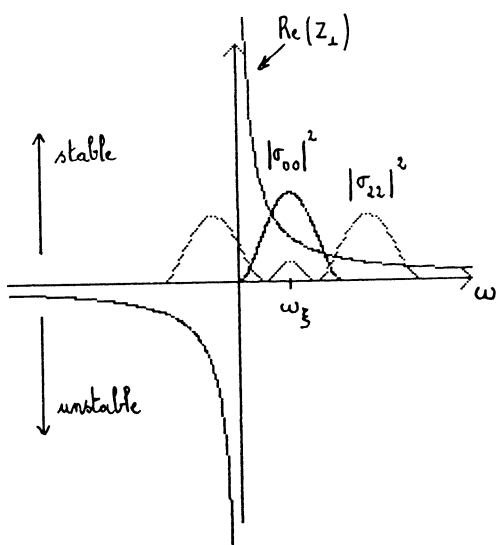


Fig. 31 Stabilisation of resistive-wall instability by chromaticity for modes $m = 0$ and $m = 2$

a) First, one can consider the effect of the short range wake (broad band type effect). This is equivalent to replacing the discrete line spectrum by a continuous spectrum. A slightly positive value of ω_ξ is sufficient in order to stabilize mode oo , but it can be seen that mode 22 for instance is unstable and the reason is evident in Fig. 31. For ω_ξ sufficiently large, both modes are damped. On the other hand, a more realistic picture of the impedance would take into account the additional damping provided by the broad band resistance. This last contribution is very efficient for stabilizing high-order modes with short bunches. As a conclusion, a slightly positive value of ω_ξ is required to get rid of the short-range wake effect.

b) Then, one can consider the effect of the long-range wake (narrow band type effect). In Fig. 32, mode oo is shown with a small ω_ξ value and Q just below an integer. Here a single line, namely the line $\omega_{R.W.} = (p+Q)\omega_0$ nearest the origin in the narrow band region of $Z_1(\omega)$, contributes to antidamping. From equation (190), one can calculate the effect.

$$\omega_c = \frac{eI}{4\pi m_e c \gamma Q} \int Z_1(\omega_{R.W.}) F_0 \left((\omega_\xi - \omega_{R.W.}) \frac{\tau_L}{2} \right) \quad (193)$$

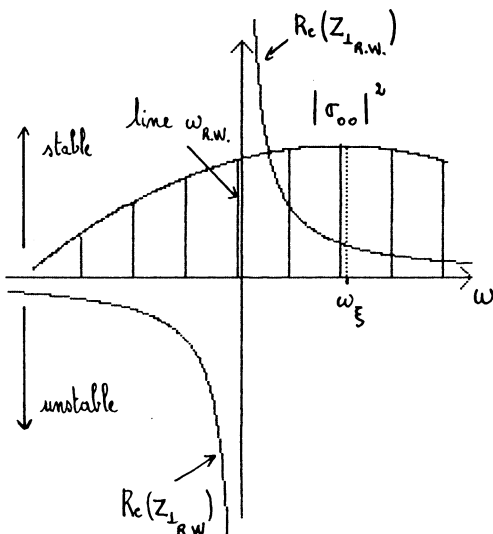


Fig. 32 Long-range effect of resistive-wall impedance for a short bunch

On the other hand, when the transverse tunes are chosen just above an integer, the long range wake has a stabilizing effect. Indeed, for multibunch operation, coupled bunch modes must be considered. The frequency shift (193) is M times larger.

Above transition, the necessity of correcting the chromaticity of the machine (strong sextupoles for sophisticated optics), gives rise to the difficult problem of dynamic aperture.

3.8.4 Stability criterion

A spread in betatron frequencies can Landau damp the instability. Let δS_1 be the within bunch full width half high spread, then, stability requires that

$$\delta S_1 > |\Delta\omega_{c_m}|. \quad (194)$$

3.9 Single-bunch instability at high intensity

The theory that has been developed in the previous sections is in quite good agreement with experiments. At low intensity, the frequency shift formulae have been extensively checked and the predicted bunch shape oscillations are commonly observed.

However, at this stage, this theory cannot predict the fast single-bunch instability that has been found in some storage rings (in PETRA, Hamburg, first).

In order to explain "Petra instability", and in analogy to the longitudinal "turbulence", R.D. Kohaupt has implemented the theory by considering transverse "mode coupling".

The basic mechanism is of the same type as the one described for the longitudinal case. We consider the most general perturbation (equation (162)) with several values of m . When the intensity gets sufficiently large for the coherent frequencies of two adjacent modes to merge, instability appears.

3.9.1 Matrix equation of single-bunch modes at high intensity

The starting point is equation (180). Both sides are divided by $\int (\omega_c - m\omega_s)$ and summed over m values:

$$\sigma(l) = \frac{eI}{2m_0c\gamma Q} \sum_p \left(\int Z_{l,p} \right) \sigma(p) \sum_m \frac{1}{\omega_c - m\omega_s} \int_0^\infty J_m^{\left[((l+Q)\omega_0 - \omega_\xi) \frac{z}{2} \right]} J_m^{\left[((p+Q)\omega_0 - \omega_\xi) \frac{z}{2} \right]} j_0(z) dz. \quad (195)$$

Let us use matrix notation.

$$\sigma(l) = \epsilon \sum_p \left(\int Z_{l,p} \right) M_{l,p} \sigma(p) . \quad (196)$$

When assuming a water-bag bunch, the matrix element $M_{l,p}$ has the following form,

$$M_{l,p} = \nu B \sum_m \frac{1}{\frac{\omega_c - m}{\omega_s}} \int_0^1 J_m^{\left[((l+Q)\omega_0 - \omega_\xi) \frac{z}{2} \right]} J_m^{\left[((p+Q)\omega_0 - \omega_\xi) \frac{z}{2} \right]} u du \quad (197)$$

while the intensity parameter ϵ is given by

$$\epsilon = \frac{eI}{4\pi m_0 c \gamma Q B \omega_s} . \quad (198)$$

In order to solve equation (196) one can proceed as follows :

Assume a real coherent betatron frequency shift measured in incoherent synchrotron frequency unit, ω_c/ω_s .

Look for the eigenvalues of the matrix

$$\left[\int Z_{l,p} \right] \cdot [M_{l,p}] \quad (199)$$

where $\left[\int Z_{l,p} \right]$ is the diagonal matrix of the impedance.

Scale the intensity parameter ϵ in order to adjust the eigenvalue to unity.

In the next two sections, we apply this method to two types of impedances, inductive wall or space charge, and broad band resonator.

3.9.2 Space-charge and inductive-wall modes at high intensity

Since there is no resistance in the assumed impedance, on one hand the frequency shifts are real (stability), on the other hand, odd and even perturbations cannot couple as already explained in section 2.8.1.

Results are gathered in Fig. 33 with ω_c/ω_s along the vertical axis and $-\epsilon(\sqrt{Z_1(p)})$ along the horizontal axis. With such a convention, inductive wall (space charge) corresponds to positive (negative) abscissas.

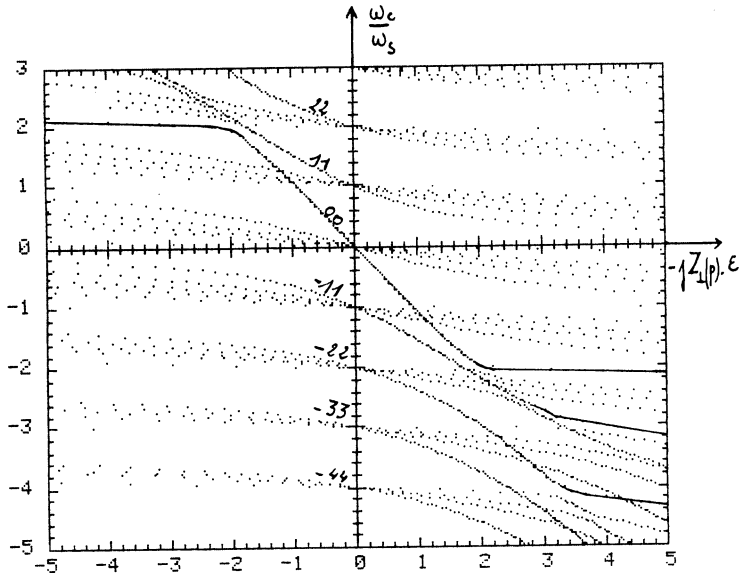


Fig. 33 Transverse coherent-frequency shift versus intensity parameter for a long bunch in an inductive impedance

At low intensity, the infinity of modes with the same m value cluster near the unperturbed frequency $m\omega_s$. The slope of the different curves is directly related to the C_{mq} 's (equation (183)).

For increasing current, let us follow continuously the curve corresponding to mode oo . Till ω_{co}/ω_s reaches ± 2 , the frequency shift is proportional to the current. Then, at higher current, because of coupling with modes of the same parity, $m=2$ or $m=-2$, the coherent frequency remains constant.

The same qualitative remarks are valid for mode 11 when considering a space charge impedance. On the contrary, when considering inductive wall, a very non linear dependence with intensity is observed. The effective high intensity frequency shift is much less than expected when extrapolating low intensity formula.

3.9.3 Broad band impedance

We assume a broad band transverse impedance

$$Z_1(\omega) = \frac{R_L \frac{\omega_r}{\omega}}{1 + j Q^* \left(\frac{\omega}{\omega_r} - \frac{\omega_r}{\omega} \right)} \quad (200)$$

with $Q^* = 1$, $\omega_r = \frac{c}{b}$ ($f_r \sim 1 \text{ GHz}$)

$$\text{and } R_L \sim \frac{2c R_S}{b^2 \omega_r} \quad (201)$$

when (165) is assumed.

Furthermore, we suppose that the chromaticity has been corrected $\omega_\zeta = 0$ as was already the case in the previous section.

Then, provided the bunch length is not extremely short ($p_b B = \omega_r \tau_L / 2\pi \gtrsim 1$), the coherent frequency of mode oo is pushed down by the inductive part of the broad-band impedance. A good estimate of ω_{co} can be found by using equation (183) and by assuming that the inductance is constant over the spectrum of mode oo .

$$\frac{\omega_{coo}}{\omega_s} = \frac{eI}{4\pi m_e c \gamma Q B \omega_s} C_{oo} \left[\int Z_{L(0)} \right] = \epsilon C_{oo} \left[\int Z_L(\epsilon) \right] \quad (202)$$

with $\int Z_{L(0)} = -\frac{R_L}{Q^*} = -R_L$ and $C_{oo} = 1.1$.

On the other hand, the coherent frequencies of the modes mq with $m = -1$ and $q = 1, 3, 5, \dots$ are pushed up or pushed down depending whether their spectrum, peaked at $\omega \sim (q+1)\pi/c_L$, overlaps a frequency region where the broad band impedance is mostly capacitive or mostly inductive.

The lowest instability threshold will occur when the coherent frequency of mode oo and the coherent frequency of one of the modes mq (with $m = -1$ and $q = 1, 3, 5, \dots$) merge. Since the frequency shifts of the modes belonging to the $m = -1$ family are weak, their coherent frequencies remain clustered near $-\omega_s$ and the lowest threshold can be approximated by

$$\frac{\omega_{coo}}{\omega_s} = -1.$$

That is to say

$$\epsilon_{th} C_{oo} \frac{R_L}{Q^*} = 1 \text{ or } \epsilon_{th} Z_{L(\omega_s)} = \frac{Q^*}{C_{oo}} \sim 9$$

or

$$\epsilon_{th} = \frac{4\pi B Q \omega_s E/e}{c R_L \frac{C_{oo}}{Q^*}} = \frac{4\pi B Q \omega_s E/e}{c R_L} \quad (203)$$

Three examples with $Q^* = 1$ are given hereunder.

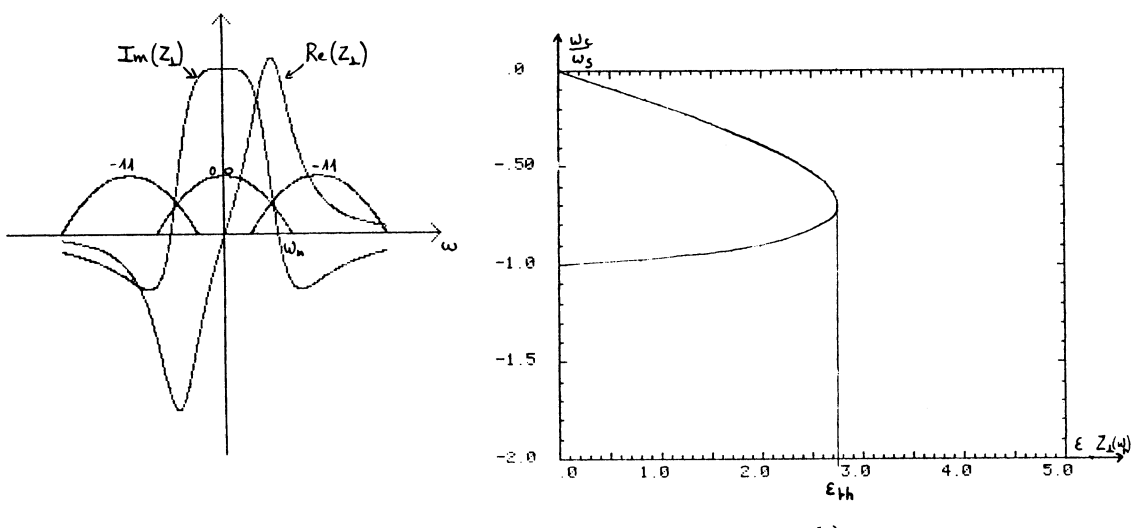


Fig. 34 Mode coupling for a very short bunch in a broad-band resonator impedance (normalized bunch length $p_T B = 0.2$)

In the first case, we are considering a very short bunch $p_T B = 0.2$ (Fig. 34a). With respect to the assumption made above, the effective C_{oo} ($C_{oo}^* = 0.2$) is much smaller than 1.1 because the tails of the frequency spectrum of mode oo extend in the capacitive region. Accordingly, the threshold is higher $\epsilon_{th} \sim 2.75$ (Fig. 34b). It corresponds to a coupling between mode oo and mode $-1 1$.

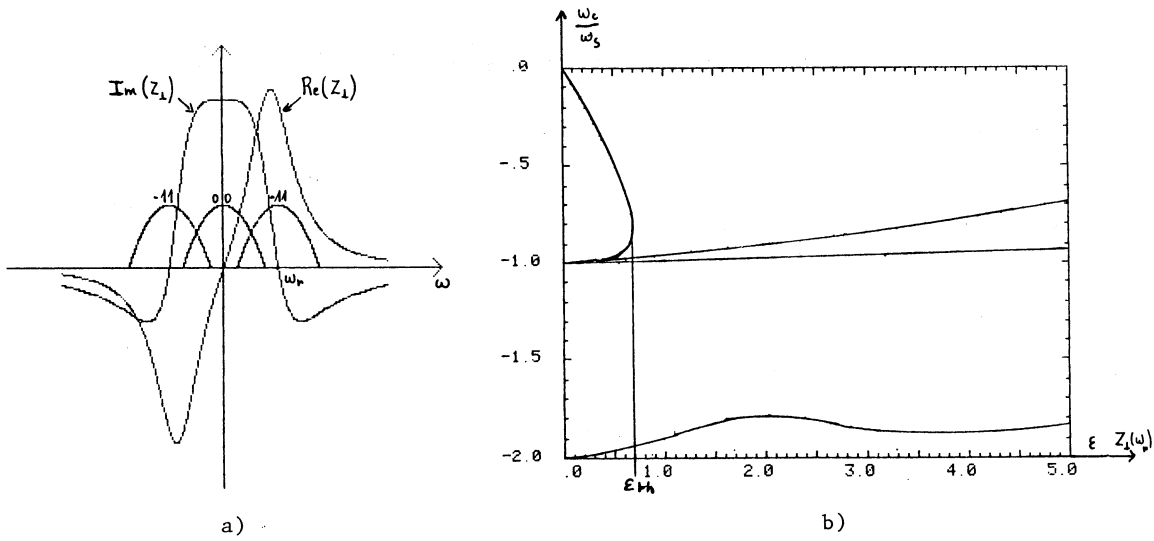


Fig. 35 Mode coupling for a bunch in a broad-band resonator impedance (normalized bunch length $p_r B = 0.8$)

In the second case, $p_r B = .8$ the effective C_{oo} is about 1.1 (Figs. 35a and 35b). On the other hand, the effective C_{-11} is about zero. Coupling between modes oo and -1 1 occurs again at $\epsilon_{th} \sim .7$ this time. This example corresponds to the worst situation. It leads to a threshold somewhat lower than foreseen before simply because the frequency shift due to the resistance has been neglected in our previous estimation.

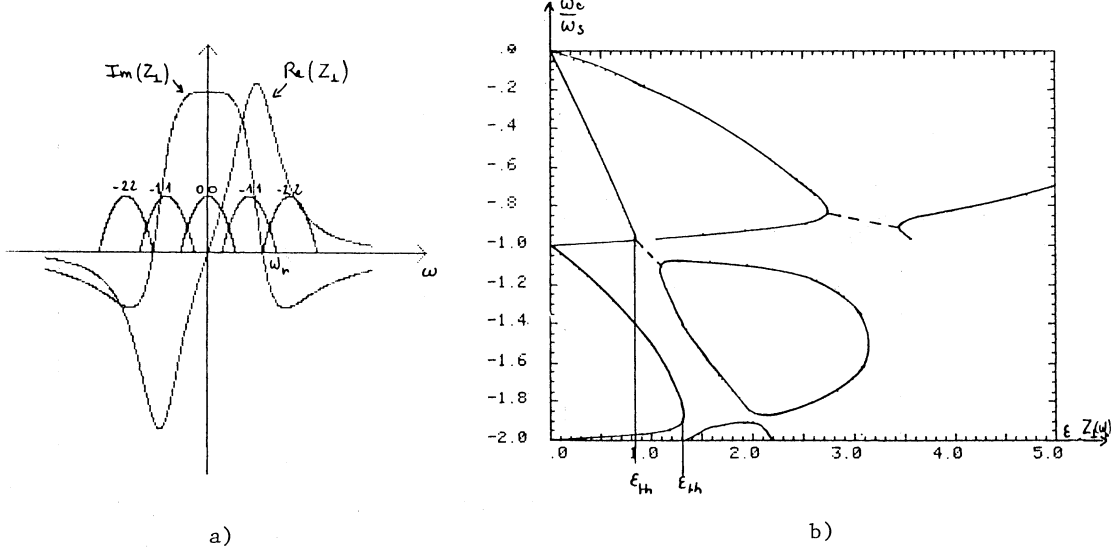


Fig. 36 Mode coupling for a long bunch in a broad-band resonator impedance (normalized bunch length $p_r B = 1.9$)

In the third case (Figs. 36a and 36b), the bunch is long $p_r B = 1.9$, and several thresholds are found. When compared to the previous cases, this time the coherent frequency of mode -1 1 is pushed down towards ω_s and mode -11 does not couple with mode oo but with mode -22 at $\epsilon_{th} \sim 1.3$. This coupling between the two most coherent modes of two successive families $m = -1$ and $m = -2$ is strong as could be seen when considering the imaginary part of ω_c . A lower threshold is found at $\epsilon_{th} \sim 0.8$. It corresponds to the coupling between mode oo and mode -13. The instability is rather weak since there is little overlap between these two modes in the region where the resistance is large.

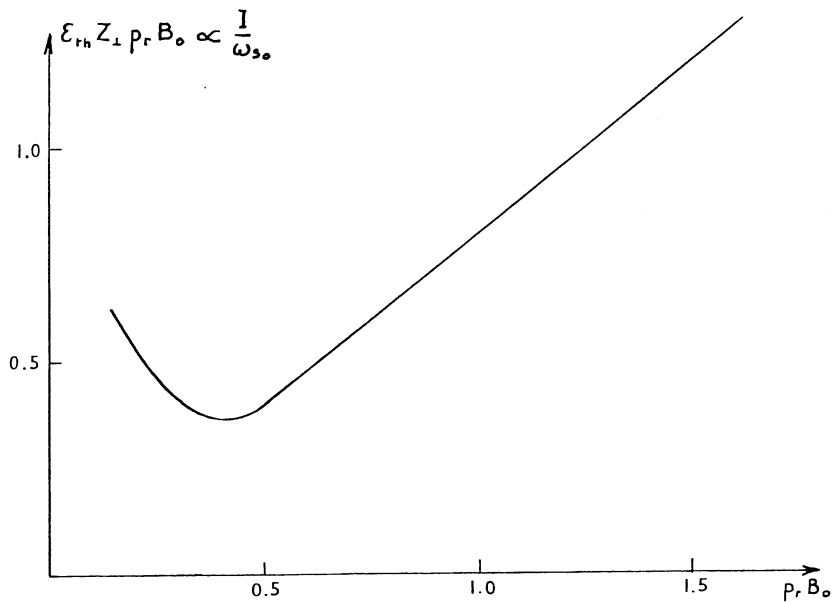


Fig. 37 Normalized threshold intensity as a function of the normalized bunch length

Results are summarized in Fig. 37. A broad band ($Q^* = 1$) impedance at resonant frequency $\omega_r = p_r \omega_0$ is assumed.

For extremely short bunches ($p_r B \approx .2$) the threshold is high. The minimum ($\epsilon_{rh} \approx .7$) is found for $p_r B \approx .8$, in rather good agreement with equation (203).

For long bunches ($p_r B > 1$) the lowest threshold is still at about the same level ($\epsilon_{rh} \approx .8$). Nevertheless, it corresponds to a rather weak coupling. Strong mode coupling occurs at higher intensity.

4. CONCLUSION

This lecture covers most of our present understanding of longitudinal and transverse coherent instabilities of bunched beams.

It seems that experimental results can be qualitatively explained by the extended F. Sacherer theory.

Quantitatively, we have insufficient knowledge of the effective coupling impedance of a machine.

ACKNOWLEDGEMENTS

This manuscript has been written in close collaboration with T. Aniel and J.P. Garnier from L.N. Saturne. A large part of the material presented here is directly drawn from the thesis prepared by J.P. Garnier.

I am very grateful to both of them for their efficient help.

I wish to thank G. Besnier for reading the manuscript and for raising several problems.

As far as references are concerned, I have proposed some of the basic ones, that look quite fundamental in order to illustrate F. Sacherer's theory. In advance, I apologize for having omitted many other valuable contributions to the subject.

REFERENCES

Longitudinal instability

- 1) F. Sacherer, Ph.D Thesis UCRL-18454 (1968).
- 2) F. Sacherer, CERN/SI/BR 72-5 (1972).
- 3) F. Sacherer, Trans. IEEE NS-20 (1973).
- 4) F. Sacherer, Trans. IEEE NS-24 (1977).
- 5) F. Sacherer, CERN/PS/BR/ 77-5 (1977).
- 6) B. Zotter, CERN/ISR/TH/ 78-9, 16(1978).
- 7) B. Zotter, CERN/ISR/TH/ 80-03 (1980).
- 8) B. Zotter, CERN/SPS/ 81-14, 18, 19, 20 (1981).
- 9) G. Besnier, B. Zotter, CERN/ISR/TH/ 82-17 (1982).
- 10) G. Besnier, Nucl. Inst. Meth. 164 (1979) 235, also Thesis, Faculté de Rennes (1978).
- 11) K. Robinson, report CEAL 1010 (1964).
- 12) E. Keil, W. Schnell, CERN/ISR/TH/RF/ 69-48 (1969).
- 13) D. Boussard, CERN/LAB II/RF/ 75-2 (1975).
- 14) T. Suzuki, Y. Chin and K. Satoh, Part. Accelerators, 13, 179 (1983).
- 15) A. Hofmann, Proc. of the Int. School of Part. Acc., Erice (1976) p. 139, CERN 77-13.
- 16) A. Hofmann. Proc. of the SLAC Summer School on Phys. of High Energy Particle Accelerators, Stanford, 1982, (AIP, New York, 1983).
- 17) A.W. Chao, Proc. of the SLAC Summer School on Phys. of High Energy Particle Accelerators (1984) p. 353.
- 18) S. Chattopadhyay, Proc. of the BNL/SUNY Summer School on Phys. of High Energy Particle Accelerators (1983) p. 467.
- 19) P.J. Channel. Proc. of the 12th Int. Conference on High Energy Accelerators, Batavia, 1983 (FNAL, Batavia, IL, 1983), p. 276.
- 20) J.L. Laclare, Proc. of the 11th Int. Conference on High Energy Accelerators, Geneva, 1980 (Birkhäuser, Basle, 1980), p. 525.

Transverse instability

- 1) C. Pellegrini, Nuovo Cimento 64A, 477 (1969).
- 2) M. Sands, SLAC-TN-69/8 and 69/10 (1969).
- 3) F. Sacherer, CERN/SI/BR/ 72-5 (1972).
- 4) F. Sacherer, CERN/PS/BR/ 76-21 (1976).
- 5) F. Sacherer, Proc. of the Int. School of Part. Acc., Erice (1976).
- 6) B. Zotter, CERN/ISR/TH/ 82-10 (1982).
- 7) B. Zotter, CERN/LEP/TH/ 85-06 (1985).
- 8) D. Brandt, B. Zotter, CERN/LEP/TH/ 83-42 (1983).
- 9) G. Besnier, D. Brandt, B. Zotter, CERN/LEP/TH/ 84-11 (1984).
- 10) Y.H. Chin, CERN/SPS/ 85-02 (1985).
- 11) R.D. Kohaupt, DESY report 80/22 (1980) and Proc. of the 11th Int. Conference on High Energy Accelerators, Geneva, 1980 (Birkhäuser, Basle, 1980), p. 562.